MOBILITY OF THE IMIDAZOLATE LINKERS IN NEAT AND CONFINED ZIFS PROBED BY ^{2}H NMR

A Dissertation
Presented to
The Academic Faculty

by

Erkang Zhou

In Partial Fulfillment
of the Requirements for the Degree
Master of Science in the
School of Chemical & Biomolecular Engineering

Georgia Institute of Technology
December 2017

MOBILITY OF THE IMIDAZOLATE LINKERS IN NEAT AND CONFINED ZIFS PROBED BY ^{2}H NMR

Approved by:

Dr. Ryan P. Lively, Advisor
School of Chemical and Biomolecular Engineering
Georgia Institute of Technology

Dr. Krista S. Walton
School of Chemical and Biomolecular Engineering
Georgia Institute of Technology

Dr. J. Carson Meredith
School of Chemical and Biomolecular Engineering
Georgia Institute of Technology

Date Approved: [November 9th, 2017]

To my parents and my son, Hong Zhou and Qinxia Pu, Aaron Ziwen Zhou

天道下济而光明 地道卑而上行

天道亏盈而益谦 地道变盈而流谦

鬼神害盈而福谦 人道恶盈而好谦

-易经

Hexagram 15: Modesty creates success.

-Classic of Changes

ACKNOWLEDGEMENTS

Time flew by, and I was surprised to find this four years of graduate school at Georgia Tech passed by imperceptibly. My emotions were mixed as I realized I was leaving the Lively Lab, a group of knowledgeable colleagues, friends, and family.

First and foremost, I must truly thank my advisor Professor Ryan P. Lively for his guidance and endless support throughout my graduate studies. His enthusiasm towards science, strong work ethic, and relentless dedication has inspired me during graduate school and beyond. He has been not only an academic supervisor, but also a life mentor. His encouragement and constant positivity has been like a lighthouse to guide me through the toughest part of my life. I will never forget the encouraging words from Boss when I was desperate "Erkang, I want you to be successful!"

The whole Lively Lab has been a pleasure to work with. Everyone in this team deserves my appreciation. I want to especially thank Brian Pimentel and Melinda Jue for the endless guidance and assistance throughout the entire four years. Technical support from Dr. Johannes Leisen is highly appreciated. I would also like to thank my committee members: Professor Krista Walton and Professor Carson Meredith for their valuable time and insights. Special credits go to Dr. Chen Zhang for taking care of me, both technically and non-technically.

TABLE OF CONTENTS

LIST OF TABLES

LIST OF FIGURES

SUMMARY

Significant work is being devoted to the reduction of global energy consumption associated with industrial separations, with increasing attention being focused on membrane technology. Zeolitic imidazolate frameworks (ZIFs) contained mixed matrix membranes (MMMs) containing are an attractive alternative to conventional thermal separation process. Framework flexibility plays a significant role in separation performance in neat ZIFs (free standing ZIFs) as well as confined ZIFs (incorporated in polymer matrix). However, the interaction between the ZIF fillers and polymer matrix remains unclear, which may be a critical factor in the design of ZIF-loaded MMMs with commercially attractive diffusion and sorption properties.

The overarching goal of this research is to understand the polymer confining effects on the motion of imidazolate linker in polymer confined ZIF fillers. By means of ^{2}H solid-state NMR techniques, imidazolate linker rotations in isotopically-enriched d-ZIF-7, d-ZIF-8, and d-ZIF-11 in free-standing and Torlon® confined environments were studied. All three d-ZIFs have very mobile linkers with a positive temperature dependency, while d-ZIF-8 exhibited the largest amplitude of linker rotation and d-ZIF-7 displayed the smallest amplitude of the rotational motion. In addition, polymer confinement effects do not change the amplitude of this rotation; meanwhile, the polymer compressive force lowered the activation energy of linker rotations in d-ZIF-11, which indicate the linker flips more often in a polymer confined environment. Eventually, polymer confining effects on transport

properties of ZIF-loaded MMMs were studied through volumetric dosing and pressure decay system and isochoric permeation system. A reduction in the sorption coefficient of ZIF confined in polymer matrix was observed, which could be a result of polymer rigidification around the ZIF crystal, or a slight reduction of in ZIF crystal unit cell volume as a result of compression from the polymer matrix. In addition, smaller transport diffusion coefficients in polymer confined ZIF-11 are observed compare to pure ZIF-11, which directly proves that imidazolate linker tends to flip more often under polymer confinement probed by solid-state NMR.

CHAPTER 1. INTRODUCTION

1.1 Background on Membrane-Based Separation

There are many challenging gas and organic liquid separations in various manufacturing pathways throughout industry. Just to give an example of the scale of some of these processes, olefin/paraffin separations are conventionally achieved by fractional distillation, which requires large amounts of thermal energy due to the low relative volatility difference between the molecular pairs. Indeed, as many as 300 trays and high reflux ratio (12-20) are required for a C3 splitter to efficiently separate propylene from propane (relative volatility ~ 1.055) [1]. Per the U.S. Department of Energy, C3 splitting is the most energy intensive single distillation in the country [2]. The large energy expense and capital investment provide the incentive to develop energy-efficient alternative separation technologies.

Membrane separations are an attractive alternative to conventional thermal separation processes due to advantages associated with energy-efficiency, compactness, and flexibility [3]. A simplified schematic of membrane-based gas separation processes is illustrated in Figure 1.1.

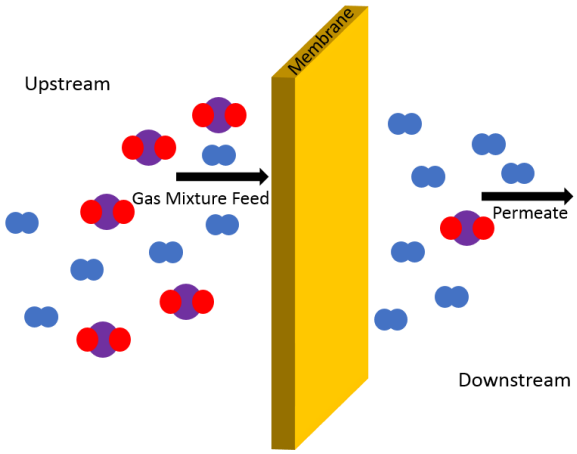

Figure 1.1: Flow scheme of membrane-based separation process.

1.1.1 Fabrication of ZIF Inorganic Membranes

Zeolitic imidazolate frameworks (ZIFs), a subclass of the metal organic frameworks (MOFs), are porous materials formed by metal centers and imidazole linkers. ZIFs received considerable attention due to their good thermal and chemical stability, as well as attractive adsorption and diffusion properties [4]. Not surprisingly, ZIFs have shown potential as materials forming inorganic membranes for separations [5-9].

Ideally, ZIF membranes would be thin films of continuous self-supporting material. However, real ZIFs are not sufficiently mechanically stable to be self-supporting and have been synthesized on different supports, including common inorganic and organic supports that are porous to provide mechanical stability and minimize resistance to mass transport [10-13]. Synthesis of these dense membranes is achieved through a variety of techniques adapted from homogeneous synthesis [3]. ZIF inorganic membranes exhibit superior separation performance with good thermal and chemical stabilities; however, their use at

industrial scales is likely limited because of the complicated fabrication process and challenge associated with scale up.

1.1.2 Applications of Polymeric Membranes

Membrane pioneers have also investigated polymeric membrane-based separations for several decades. Polymeric membranes are relatively inexpensive and easy to fabricate and scale up. Typically, polymers selected to fabricate membranes need good chemical, thermal, and mechanical stabilities under aggressive feed conditions such as high temperature, high pressure, humidity, and aggressive gas mixtures [3]. In addition, polymers should exhibit both high gas permeability and selectivity to become attractive for targeted industrial applications. However, Robeson observed there is permeability and selectivity trade-off relationship (Robeson upper bound) of polymeric membranes [14, 15], which limits their utility in demanding separations.

1.2 ZIF-loaded Mixed Matrix Membranes

Mixed matrix membranes (MMMs) as shown in Figure 1.2, consisting of a non-polymeric separating agent (discrete phase) and an easily processable polymer (continuous phase), have been proposed to overcome material limitations associated with both materials [16]. These membranes have been studied for approximately 50 years since Barrer and James first demonstrated the concept [17, 18]. Interest has grown in the incorporation of ZIFs into polymeric matrices, which are commonly referred to as ZIF-loaded mixed matrix membranes (or ZIF MMMs) [19-25]. These can potentially enable excellent separation performance as well as an economical fabrication process.

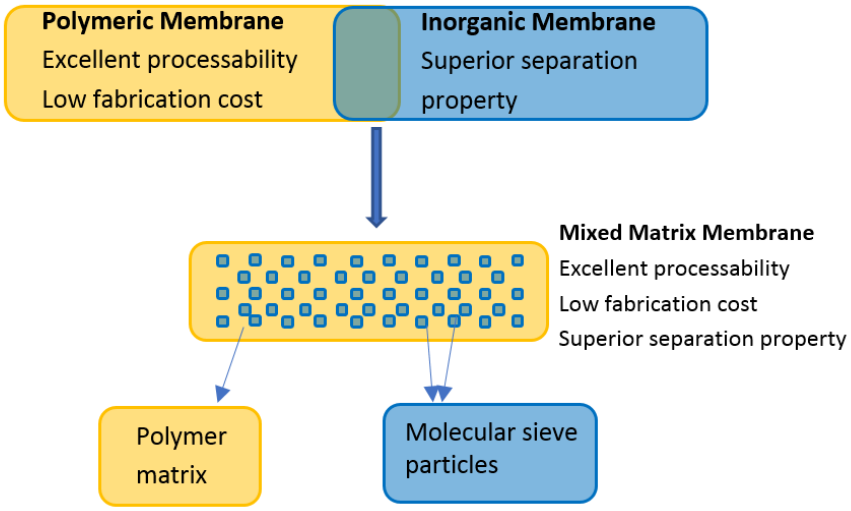

Figure 1.2: Scheme of Mixed Matrix Membranes.

1.2.1 Fabrication of ZIF-loaded Mixed Matrix Membranes

There are numerous combinations of ZIF fillers and polymeric matrices; however, the fabrication procedure of ZIF-loaded MMMs is in general similar [3, 26]. Typically, ZIF particles and polymer powders are separately dispersed in organic solvents (e.g., dichloromethane, chloroform, and tetrahydrofuran) via alternating stirring and sonication. To help prevent aggregation and enhance interactions between the polymer matrix and the ZIF fillers, ZIF crystals are usually "primed" or pre-coated with a thin layer of polymer by adding a small amount of dilute polymer solution via stirring and sonication treatments [27]. The remaining polymer solution is added to the ZIF particle suspension followed by several alternating stirring and sonication treatments until a homogeneous soliton is formed. After MMM casting solution preparation, standard knife casting techniques are normally applied. Overall, the MMM fabrication procedure is largely similar to that of zeolite-loaded MMMs with the exceptions that the ZIFs typically do not need surface

functionalization to promote adhesion to the polymer and the need to account for the reduced chemical stability of ZIFs relative to zeolites.

1.2.2 Transport in ZIF-loaded Mixed Matrix Membranes

Transport through dense membranes (including MMMs) can be described by the sorption-diffusion model. Gas molecules first dissolve at the upstream of the membrane and diffuse through the membrane along a chemical potential gradient, and eventually desorb at the downstream. Permeability is the pressure difference and membrane thickness normalized flux as shown in equation (1.1), which describes the membrane's intrinsic productivity.

$$P_i = \frac{N_i * l}{\Delta p_i} \tag{1.1}$$

Where N_i is the steady-state flux, l is the membrane thickness, and Δp_i is the partial pressure difference in the case of ideal gases. Permeability is usually given in the unit of Barrer:

$$1 \text{ Barrer} = 1 \times 10^{-10} \frac{cc(STP) \cdot cm}{cm^2 \cdot s \cdot cmHg}$$

The permeability of the penetrating molecule can be written as the product of diffusivity and sorption coefficient [28]:

$$P_i = D_i \times S_i \tag{1.2}$$

Where D_i is the diffusivity, and S_i is the sorption coefficient. The sorption coefficient can be expressed by equation (1.3):

$$S_i = \frac{C_i}{p_i} \tag{1.3}$$

Where C_i is the sorption uptake obtained from equilibrium isotherms. The permselectivity of a membrane material, $\alpha_{A/B}$, is a measure of a membrane's ability to differentiate between guest molecules A and B and is given by the ratio of permeabilities, which can be further expressed as equation (1.4):

$$\alpha_{A/B} = \frac{P_A}{P_B} = \left(\frac{D_A}{D_B}\right) \times \left(\frac{S_A}{S_B}\right) \tag{1.4}$$

Where (D_A/D_B) is the diffusion (kinetic) selectivity, (S_A/S_B) is the sorption (thermodynamic) selectivity.

Gas sorption in glassy polymers and ZIF fillers can be characterized by the dual mode model and Langmuir model, respectively. Moreover, the diffusion coefficient decreases as molecule size of gas increases in polymer matrix because penetrant gas molecules must make a localized diffusion step when a transient opening in the polymer matrix occurs due to thermal fluctuations. On the other hand, gas molecules diffuse in ZIF fillers by random jumps through those interconnecting channels that connect large cavities of the material.

Typically, the Maxwell model [29] is employed to describe the gas transport in ZIF-loaded MMMs, which is expressed by equation (1.5):

$$P_{ZIF-MMM} = P_p\left[\frac{P_{ZIF}+2P_p-2\varphi_{ZIF}\left(P_p-P_{ZIF}\right)}{P_{ZIF}+2P_p+\varphi_{ZIF}\left(P_p-P_{ZIF}\right)}\right] \tag{1.5}$$

Where $P_{ZIF-MMM}$ is the permeability in ZIF MMM, P_p is the permeability in the polymer matrix, P_{ZIF} is the permeability in ZIF particles, and φ_{ZIF} is the volume fraction of ZIF particles in the MMM.

1.2.3 Challenges associated with ZIF-loaded Mixed Matrix Membranes

Typically, the design of ZIF MMMs assumes the independence of the transport, sorption, and related structural properties of ZIF crystals in and out of the polymer-confined environment [30, 31]. In addition, there is experimental evidence suggesting that the framework flexibility of ZIF particles has a significant influence on the transport and sorption properties of these materials [26, 30, 32]. In approximating the structure of ZIF particles, the flexible structure is typically time-averaged as shown in Figure 1.3 [33]. Neglecting the effect of the large tail of the time-averaged distribution may lead inaccuracy of the prediction due to the significant role in diffusion it plays. For instance, ZIF-8 with a time-averaged window size distribution has a mean pore window size of 3.38 Å, which can exclude larger molecules; however, there is substantial experimental evidence showing that ZIF-8 can surprisingly let larger guest molecules diffuse through the framework [30, 34]. In addition, a recent work reported by Sholl and co-workers showing that the pore size of ZIF-8 crystals is highly dependent on the adsorbate positioned in the pore window [35].

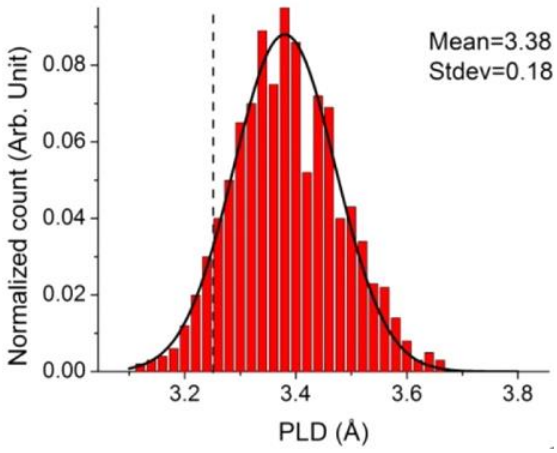

Figure 1.3: Histograms of the PLD distributions from AIMD simulations for ZIF-8 [33].

In addition, recent work highlighted the dependence between diffusion and sorption properties of ZIFs and the polymer matrix providing the confined environment. For instance, Caro and coworkers observed dramatically increased H_2/CH_4 selectivity from Matrimid® coated ZIF-8 and ZIF-90 membranes [36]. Li and coworkers also observed significantly enhanced C3 selectivity from PDMS coated ZIF-8 membranes [37]. Lower ethylene diffusivities of ZIF-8 are obtained through PFG-NMR when the crystals are confined in 6FDA-DAM polymer matrix, as reported by Vasenkov and coworkers [38].

We hypothesized that the residual stress in the polymer matrix as a result of solvent loss and subsequent transition from rubbery to glassy polymer exerts an isotropic stress on the ZIF on the order of 3000 atm. In Figure 1.4, the top part illustrates the origin of isotopic stresses around polymer-confined ZIFs. We hypothesized that the polymer-confined ZIF would exhibit a decrease in the rotational mobility of imidazolate ligands, which results in a decrease in gas self-diffusivity through the polymer-confined ZIFs relative to the neat ZIFs. As shown in the middle part of Figure 1.4, idealized here as the rotational flexibility of the imidazolate ligands, shown as the black arms-as a result of confinement within a polymer matrix. The bottom part of Figure 1.4 shows the hypothesized change in polymer chain packing as a result of mixed matrix membrane formation. This work aims at quantifying the relation between material microstructure and mass transport properties through the hybrid material.

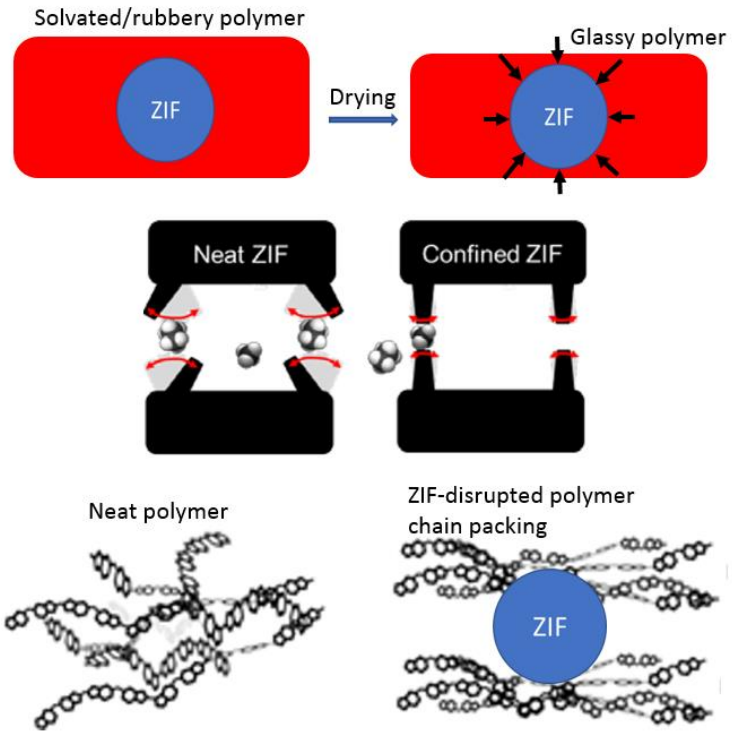

Figure 1.4: Overview of reduction in ZIF framework flexibility.

1.3 Background on Soild-State Nuclear Magnetic Resonance

^{2}H NMR spectroscopy is a powerful technique that can be adapted to investigate the nature of molecular motion in solid materials. The technique is generally used under static conditions, i.e., the otherwise common magic angle spinning (MAS) technique is not used. This is especially relevant for the proposed study since for MAS, which measures pneumatically spun samples, is difficult to prepare samples containing a well-defined gas loading [39]. In contrast, the ^{2}H-NMR spectroscopy technique can study samples of interest for a variety of gas-loadings. In addition, temperatures can be easily controlled under static

conditions such that ^{2}H-NMR studies over a broad temperature range (-100 °C to 150 °C) are quite common.

1.3.1 Solid Echo Lineshape Analysis

In solid-state NMR, the measurement of molecular orientations and reorientations of segments is based on the orientation dependence of NMR interactions in solids [40, 41]. The anisotropies due to the tensorial nature of the interactions reflect the orientations of molecular segments. In solids, the quantum mechanical interactions of the ^{2}H nucleus are especially simple to describe. They are dominated by the quadrupolar interaction. In most cases the ^{2}H quadrupolar tensor can be approximated by an axially symmetric tensor aligned with the axis formed by the C-^{2}H bond. The frequency of the respective transition can be described using equation (1.6) [42] and Figure 1.5.

$$\omega = \omega_0 \pm \delta_Q(3cos^2\vartheta_i - 1) \qquad (1.6)$$

Where ω_0 is the Larmor frequency of the unshielded nucleus, δ_Q is the quadrupole coupling constant.

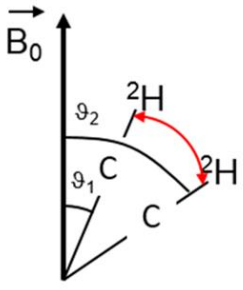

Figure 1.5: ^{2}H quadrupolar tensor expressed by an axially symmetric tensor aligned with the axis formed by the C-^{2}H bond.

δ_Q, the quadrupole coupling constant, is typically derived from equation (1.7) in the case of deuteron [42]:

$$\frac{4}{3}\delta_Q = \frac{eQeq}{h} \ (\approx 2\pi*170 \text{ kHz for aliphatic C-}^2\text{H})$$

$$(\approx 2\pi*180 \text{ kHz for aromatic C-}^2\text{H}) \qquad (1.7)$$

The orientation of the magnetic field in the principal axes system of the field gradient tensor is specified by one single angle θ depicting the orientation of the vector formed by the C-^{2}H bond with respect to the magnetic field. δ for ^{2}H in C-^{2}H bonds show a minor variation between different types of chemical bonds; often it is safe to assume a value of $\frac{\delta_Q}{2\pi}$ = 128 kHz for aliphatic C-^{2}H and 135kHz for aromatic C-^{2}H. As a result, for the above equation, the single orientation an individual C-^{2}H bond with respect to the magnetic field results in a symmetric splitting of two equivalent peaks. This is caused by + and – signs reflecting the two quantum mechanical transitions of the ^{2}H, which has a spin of 1. The presence of an ensemble of C-^{2}H bonds leads to peak patterns, reflecting the orientation of the bonds. In the case of a random orientation, the typical ^{2}H-powder pattern (Pake pattern) is observed.

Since ^{2}H NMR is able to probe the angle of individual C-^{2}H bonds with respect to a magnetic field it is also able to probe molecular motions/reorientations [43, 44]. Motions occurring with frequencies >> δ will lead to the detection of averaged frequencies, which can still be calculated using equation (1.8), while will be discussed in next section. The effect of various types of motion leads to characteristic line-shapes, which have been published. Due to the lattice nature of molecular structures, it is possible to approximate

many common molecular motions through exchange of sites defined by a cone. Those motions can be readily calculated with the software NMR-Weblab [42].

1.3.2 T_1 Relaxation Analysis

While ^{2}H-solid echo experiments measure motion via the average orientation of ^{2}H-C bonds on a timescale faster than ~ 10 kHz, measuring T_1 relaxation time provides a complementary means to study molecular motions on the time scale of MHz [45]. This relaxation is caused by fluctuating magnetic fields [46]. In the case of ^{2}H NMR, those fluctuations are largely induced via molecular motions. A common theory used to calculate correlation times from molecular motions is the Bloembergen-Purcell-Pound theory (BPP theory) as described in equation (1.8). It is typically applied to explain the relaxation constant of a pure substance in correspondence with its state and effect of the tumbling motion of molecules on the local magnetic field disturbance [47]. While this theory might give a first approximation to extract a correlation time, it should be also noted that T_1 relaxation times depend on the nature of the associated molecular motions and associated relaxation mechanisms.

$$\frac{1}{T_1} = C\left(\frac{\tau}{1+\omega_0^2\tau^2} + \frac{4\tau}{1+4\omega_0^2\tau^2}\right)$$

$$\frac{1}{T_2} = C\left(3\tau + \frac{5\tau}{1+\omega_0^2\tau^2} + \frac{2\tau}{1+4\omega_0^2\tau^2}\right) \quad (1.8)$$

Where T_1 and T_2 are spin-lattice and spin-spin relaxation time correspondingly, C is the force constant (quadrupolar coupling), τ is the molecular motion correlation time, ω_0 is Larmor frequency. By analogy with chemical kinetics, magnitude of the molecular motion correlation times τ depend on the temperature as $\tau = \tau_0 \exp(E_0/RT)$. T_1 plotted in

semi logarithmic coordinates versus the correlation time will provide a V-shaped curve as show in Figure 1.6, with a minimum for $\tau = 0.62/\omega_0$. For a thermally activated process, the activation energy E_0 can be obtained from an Arrhenius plot of the correlation time as a function of temperature.

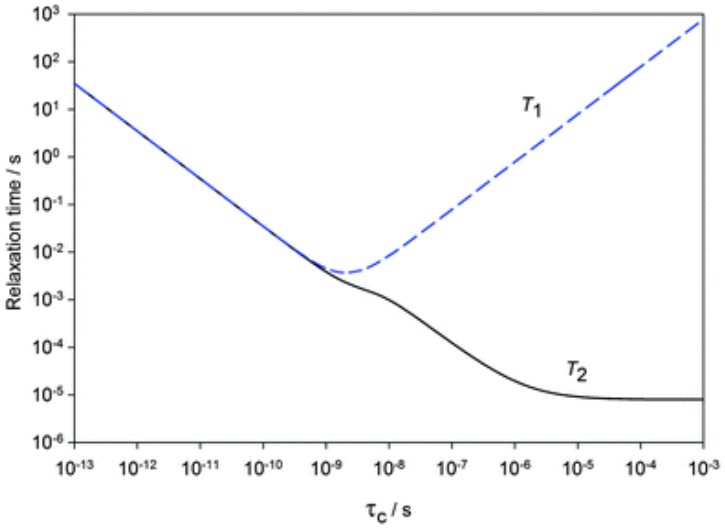

Figure 1.6: Theoretical behavior of T_1 and T_2 as a function of the correlation time τ.

1.4 Motivation and Thesis Outline

Mixed matrix membranes containing ZIF crystals are an attractive alternative to conventional thermal separation process. Framework flexibility plays a significant role in separation performance in neat ZIFs (free standing ZIFs) as well as confined ZIFs (incorporated in polymer matrix). However, the interaction between the ZIF fillers and polymer matrix remains unclear, which may be a critical factor in the design of ZIF-loaded mixed matrix membranes with commercially attractive diffusion and sorption properties.

This thesis work aimed to understand the interplay between the ZIF crystals fillers and polymer matrix in ZIF-loaded MMMs.

The main objective of this thesis work is to understand the polymer confining effects on the motion of imidazolate linker in polymer confined ZIF fillers. Moreover, the molecular dynamics (framework flexibility) of ZIF crystals in neat and confined environments has been directly studied. In addition, transport properties of such materials have also been compared to support previous findings here and in the literature. Chapter 2 of this thesis reports the synthesis of isotopically enriched ZIF-7, ZIF-8, and ZIF-11 through modified synthesis protocol. The molecular dynamics of as-synthesized isotopically enriched ZIFs were studied by solid-state NMR techniques. Chapter 3 of this thesis reports the fabrication of isotopically enriched ZIF-loaded MMMs and the study of the molecular dynamics of polymer matrix confined imidazolate linkers via solid-state NMR techniques. Chapter 4 of this thesis reports the transport and sorption properties of regular ZIF crystals in neat and confined environments through volumetric dosing adsorption and isochoric permeation system. Chapter 5 summarizes the conclusion of this thesis work with proposed future research as extension of the work.

CHAPTER 2. SYNTHESIS AND INVESTIGATION OF ISOTOPICALLY-ENRICHED ZIF7, ZIF-8, AND ZIF-11

2.1 Introduction

Zeolitic imidazolate frameworks (ZIFs), an emerging subclass of the metal organic frameworks (MOFs), are microporous materials containing imidazolate building units. The robustness of these ZIF structures with uniform microspores and high surface areas has made them attractive for numerous applications, including catalysis [48], electronic devices [49], drug delivery [50], separations, and more [3].

ZIF materials are constructed by metal ions that act as lattice nodes that are then held in place by organic ligands. Due to the wide range of metal ions (zinc, copper, cadmium, and cobalt) and organic ligands (2-methylimidazolates, benzimidazole, and more) that can be built into ZIFs, over 150 ZIF structures have been synthesized [4], as well as countless hybrid versions of these existing 150 structures. These materials enable a diverse variety of topologies and highly designable pore sizes and shapes, which endow ZIF materials with tunable cavity architectures and properties [3]. One of the most promising applications of these materials is their utilization as the selective component of membranes. For application as the selective material in a, one of the key performance metrics is well-defined frameworks with predictable molecular sieving pore window dimensions to realize sufficient selectivity in target separations. However, many experimental evidences showed that ZIF materials exhibit relatively flexible frameworks, which has significant influence

on the transport and sorption properties of guest molecules [3]. As a result, understanding the framework flexibility is critical in designing ZIF-based membranes.

In this chapter, three ZIFs are chosen for the reasons noted below. ZIF-7 with sodalite (SOD) as the framework type is formed by bridging benzimidazole (BIm) linkers with zinc ions. ZIF-7 shares the same crystal structure with sodalite zeolite, where oxygen is replaced by BIm and Si/Al is replaced by Zinc ion. ZIF-7 exhibits a relatively rigid framework due to the inability of the bulky linker to appreciably rotate around its coordination bond through relatively small pore. Framework flexibility can be understood as the thermal vibrations of the ZIF window, while gate opening represents the flipping of the imidazolate linkers into an open pore structure. On the other hand, ZIF-8 has the same SOD topology with ZIF-7, and is expected to be more flexible since 2-methylimidazole (2mIm) linker is smaller while the pore is larger. In addition to ZIF-7 and ZIF-8, ZIF-11 with RHO topology is expected to yield a relatively moderate framework flexibility due to same bulky BIm ligand but large pore diameter which allows the linkers to rotate around coordination bonds more readily than ZIF-7. As a result, ZIF-11 is expected to demonstrate framework flexibility in between that of ZIF-7 and ZIF-8.

In this study, the effects on imidazolate linker rotation induced by polymer matrix are directly investigated through solid-state NMR technology. ^{2}H NMR spectroscopy is a powerful technique that can be adapted to investigate the nature of molecular motion in solid materials, such as the detection of rates of molecular motions and the exact characterization of the geometry of the motion. For instance, ^{2}H NMR has been utilized to study the motion of molecules within zeolites, microporous silicas, polymers, and MOFs [51- 55]. In this work, the ^{2}H-NMR spectroscopy technique is utilized to study the nature

of molecular motion ZIF crystals. Due to the extremely low natural abundance of deuterium (^2H), which is at about 0.0156%, the ZIF crystals need to be isotopically enriched to enable detection.

2.2 Synthesis of Neat Isotopically-Enriched ZIF crystals

2.2.1 Synthesis of isotopically-enriched ZIF-7

Isotopically-enriched ZIF-7 (d-ZIF-7) crystals were prepared through modified solvothermal synthesis protocol reported by He et al [56]. 300 mg (2.456 mmol) Benzimidazole-4,5,6,7-d_4 (CDN ISOTOPES), was dissolved in 20 ml dimethylformamide followed by 650 µL diethylamine (Sigma-Aldrich). After 15 min of stirring, 321 mg (1.228 mmol) $ZnBr_2 \cdot 2H_2O$ (Alfa Aesar) was dissolved in 15 ml dimethylformamide. The former solution was poured into the latter solution under stirring. The precursor solution was heated at 130 ºC for 24 hours in an autoclave. The product d-ZIF-7 crystals were recovered by centrifugation, followed by extensive washing with methanol. The product was activated at 130 ºC under dynamic vacuum for 24 hours.

2.2.2 Synthesis of isotopically-enriched ZIF-8

Isotopically-enriched ZIF-8 (d-ZIF-8) crystal was prepared through modified solvothermal synthesis protocol reported by Cravillon and co-workers [57]. 844 mg (2.836 mmol) $Zn(NO_3)_2 \cdot 6H_2O$ (Alfa Aesar) was dissolved in 50 ml methanol. 500 mg (5.673 mmol) 2-Methylimidazole-d_6 (CDN ISOTOPES) and 772 mg (11.346 mmol) HCO_2Na were dissolved in 50 ml methanol. The latter solution was poured into the former solution under stirring. The precursor solution was heated at 90 ºC for 24 hours in a glass pressure

vessel. The product of d-ZIF-8 were recovered by centrifugation, followed by extensive washing with methanol. The product was activated at 130 ºC at dynamic vacuum for 24 hours.

2.2.3 Synthesis of isotopically-enriched ZIF-11

Isotopically-enriched ZIF-11 (d-ZIF-11) crystal was prepared through modified solvothermal synthesis protocol reported by He et al. [56]. 300 mg (2.456 mmol) Benzimidazole-4,5,6,7-d_4 (CDN ISOTOPES), 11.3 g (122.8 mmol) Toluene, and 147 mg (2.456 mmol NH_3) were dissolved in 40 ml methanol under stirring. After 15 min of stirring, 270 mg (1.228 mmol) $Zn(O_2CCH_3)_2 \cdot 2H_2O$ (Alfa Aesar) was added to former solution and stirred for 4 hours at room temperature. The product of d-ZIF-11 were recovered by centrifugation, followed by extensive washing with methanol. The product was activated at 130 at dynamic vacuum for 24 hours.

2.2.4 Product Characterizations

The workflow approach for this portion of the work is shown in Figure 2.1. The scheme starts from synthesizing ZIF from regular imidazole linkers. In the first route, lab-synthesized ZIF crystals with high quality that is close to the literature value are determined through X-Ray powder diffraction (XRD). Tremendous work has been focused on increasing the yield of the product before the expensive deuterated linkers are used. The isotopically-enriched ZIF crystals will then be synthesized followed by the same characterization techniques. If any test revealed undesirable properties of the ZIF crystals, the synthesis process was modified before moving onto the deuterated synthesis.

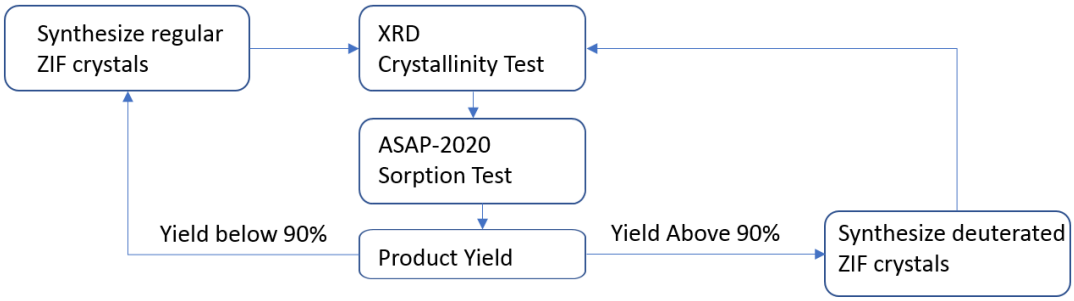

Figure 2.1: Scheme of preparing isotopically-enriched ZIF crystals.

Isotopically-enriched ZIF-7, ZIF-8, and ZIF-11 were prepared through modified solvothermal synthesis protocol available in the literature, as noted above [56, 57]. The crystalline phase of the samples was determined by X-Ray powder diffraction using X'Pert PRO PANalytical Powder Diffractometer. The integration time was 20 minutes and the step size was 0.016 degrees/second. As shown in the Figure 2.2, powder XRD patterns of as-synthesized isotopically-enriched ZIF crystals match well with simulated literature value.

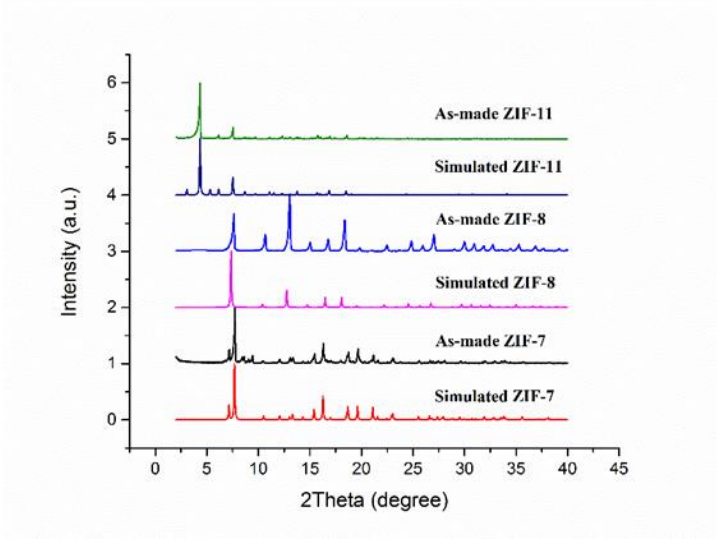

Figure 2.2: XRD patterns of synthesized d-ZIF-7, d-ZIF-8, and d-ZIF-11 compared with simulated patterns.

2.3 Solid-State NMR Experiments

2.3.1 Solid-State NMR Sample Preparation

Solid-State NMR samples were prepared by loading about 80 mg lab-synthesized d-ZIF crystal powders into 5 mm (o.d.) and 30 mm (length) Norell® NMR tube. Two open ends of the tube were sealed with PTFE thread sealant tape. The sample was kept at 130 ºC at dynamic vacuum before the test.

2.3.2 Solid-State NMR Instrument Set-up

The experiments were performed on a wide-bore 7 Tesla Bruker AV3-HD 300 NMR spectrometer with 5mm probehead with a solenoid coil optimized for ^{2}H with Larmor frequency at $\frac{\omega_0}{2\pi} = 46$ MHz and wide-bore 9.4 Tesla Bruker AV3 400 NMR spectrometer with 5 mm probehead with a solenoid coil optimized for ^{2}H with Larmor frequency at $\frac{\omega_0}{2\pi} =$ 61 MHz.

^{2}H-solid echo experiments were carried out with pulse sequence of 90^o_x-τ_1-90^o_y-τ_2-acquisition-t. For ZIF-7 and ZIF-11, the pulse length was set to be 4 μs and the delay between pulses was 30 μs, 512 scans were recorded with a repetition delay of 10s (6144 scans for ZIF-8). Spectra were Fourier transformed starting with the data point of the echo maximum after an exponential multiplication leading to a line broadening of 3000 Hz.

Spin-lattice relaxation times (T_1) were obtained through saturation recovery experiments using the pulse sequence train of pulses-VD-acquisition-train of pulses-VD'-acquisition. VD_{MAX} is set at about 5 times of T_1 so the longitudinal magnetization is

recovered completely before the next train of pulses, which FID gives the maximum signal each time. Experiments were carried through a broad temperature range, 173 to 423 K, controlled with a flow of nitrogen gas.

2.4 Results and Discussions

We first investigated the rotational dynamic motions of 2-methylimidazole within neat d-ZIF-8. The d-ZIF-8 with no linker rotation dynamics at 323K were simulated using NMR WEBLABs. The experimental dynamics of d-ZIF-8 can then be compared to the simulated Pake patterns, as shown in Figure 2.3.

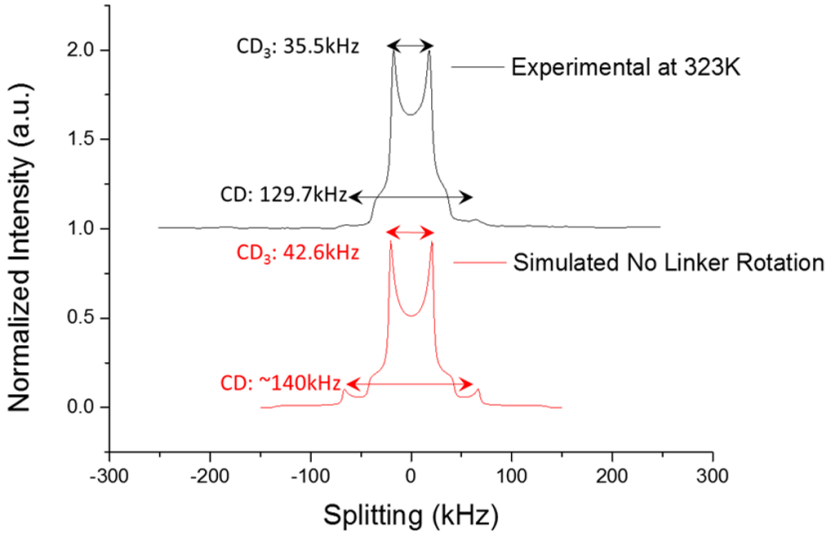

Figure 2.3: Pake Patterns of measured d-ZIF-8 and NMR WEBLAB simulated spectra with no linker rotation at 323 K.

All spectra of neat d-ZIF-8 measured at different temperatures are almost identical. Due to a direct correlation of the line shape with the type of a molecular motion, identical Pake patterns indicates that the imidazolate linkers undergo the same type of motion [58]. In d-ZIF-8, two types of motions are revealed via the two signals observed in the Pake

pattern: a strong narrow signal contributed from fast methyl group (CD_3: site 1 to 3) self-rotation and a weak broad signal expected from CD (site 4 and 5) in the imidazolate ring rotating along the N-N axis in d-ZIF-8 as shown in Figure 2.4 and Figure 2.3.

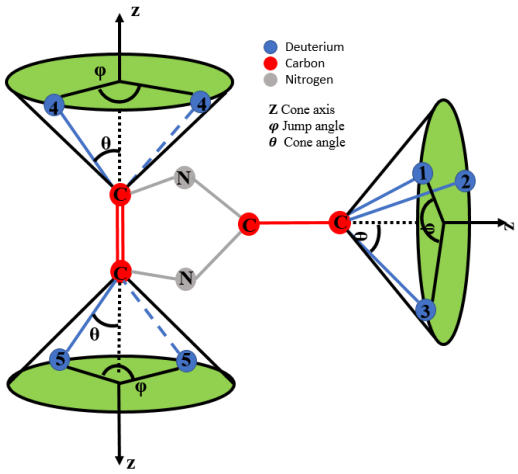

Figure 2.4: Cone mode of 2-methylimidazole linker in d-ZIF-8.

Similar ^2H NMR spectra have also been observed by Jobic and coworkers [54]. Numerical simulations [59] of the CD_3 self-rotation derives a splitting in the Pake pattern at about 42.6 kHz. Aliphatic deuteron quadrupole coupling constant (δ_0) of 128 kHz [42], cone angle (θ) of 70.5º driven by the tetrahedral CD_3 geometry, and jump angle (φ) of 120º obtained from 3 even distributed sites (CD_3: site 1 to 3) are applied in the numerical simulations. The observed CD_3 splittings in Figure 2.3 are narrower at about 35 kHz, which indicates CD_3 not only undergoes self-rotation, but also undergoes imidazolate linker rotation. In addition, caption of such motion by ^2H solid echo NMR experiment implies that imidazolate linker motion is faster than solid echo time scale (kHz).

Since CD_3 undergoes self-rotation and linker rotation simultaneously, the effect from CD_3 self-rotation should be eliminated to evaluate the extent of linker rotation. In this

case, it is safe to assume 42.6 kHz as quadrupole coupling constants [42, 54, 59] and treat CD_3 as a whole quadrupole moment in analyzing the splittings. As a result, the whole CD_3 group has a cone angle (θ) of 90º.

As plotted in Figure 2.5, CD_3 splitting decrease from 36.4 to 34.9 kHz as temperature increase from 173 to 423 K. Compared with numerical simulation, the gauss distribution for jump angle (libration angle 2σ) is found to increase from 37.7 to 42.4º over this temperature range as shown in Figure 2.6.

The weak wide signal reflects the linker rotation contributed only by 2 CD groups in the imidazolate ring. The analysis of the spectra line shape arising from the CD groups also shows an increase in the jump angle from 37 to 42º as temperature increases. Both narrow and wide splittings extracted a consistent temperature dependence (minor difference between splittings at different temperatures) on the amplitude of imidazolate linker rotations.

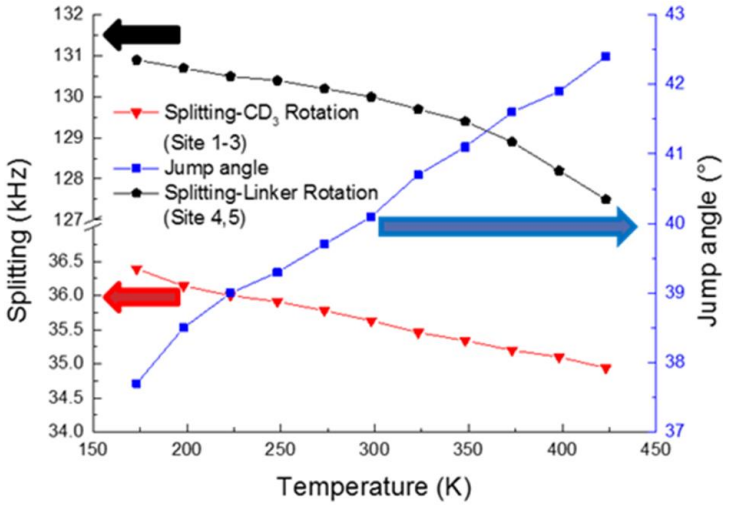

Figure 2.5: Pake splitting and jump angle of d-ZIF-8 measured from 173 to 423 K.

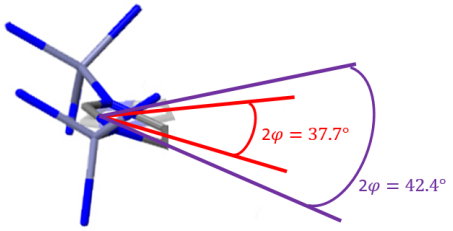

Figure 2.6: Temperature dependence of ZIF-8 linker jump angle at 173 K (red) and 423 K (purple).

The rotational dynamic motions of benzimidazole linkers in ZIF-7 and ZIF-11 are characterized by similar Pake patterns. Unlike ZIF-8 undergoes CD_3 both fast self-rotation and imidazolate linker rotation, ZIF-7 and ZIF-11 exhibit only one dynamic motion. The experimental dynamics of d-ZIF-11 measured at 323 K can be compared with the simulated Pake patterns of ZIF-11 with no imidazolate linker rotation as plotted in Figure 2.7. The experimental splitting is at about 127.7 kHz, which is narrower than 135 kHz simulated from ZIF-11without linker motion, directly proof the existence of benzimidazole linker rotations.

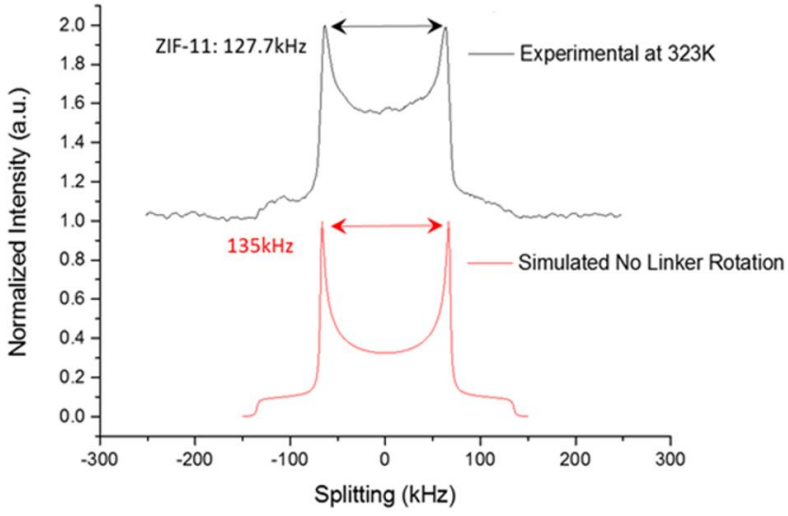

Figure 2.7: Pake Patterns of measured d-ZIF-11 and NMR WEBLAB simulated spectra with no linker rotation at 323 K.

Same as d-ZIF-11, rotational dynamic motions of linker within neat d-ZIF-7 were characterized by the splitting contributed from two CD groups in the benzene ring of the imidazolate linker. As shown in the black curve in Figure 2.7, measured splitting decrease from 130 to 128.4 kHz as temperature increase from 173 to 423 K. When comparing with numerical simulated spectra, the aromatic deuteron quadrupole coupling constant (δ_0) is applied at 135 kHz, while the cone angle (θ) is about 60º based on the geometry of benzimidazole. As plotted in the blue curve in Figure 2.8 and shown in Figure 2.9, the gauss distribution of jump angle 2σ is derived to increase from 21.3 to 24.4º as temperature increases. Linker rotation in ZIF-7 showed a consistent temperature dependence through the entire experiments.

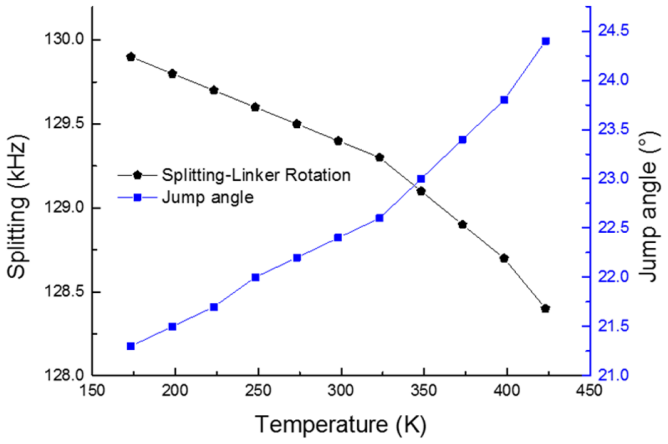

Figure 2.8: Pake splitting and jump angle of d-ZIF-7 measured from 173 to 423 K.

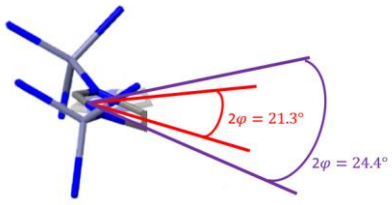

Figure 2.9: Temperature dependence of ZIF-7 linker jump angle at 173 K (red) and 423 K (purple).

Rotational dynamics motions of linker within neat ZIF-11 were characterized by similar splittings; however, a narrower splitting indicates the imidazolate linker in d-ZIF-11 is more mobile than in d-ZIF-7. As shown in the black curve Figure 2.10, the CD group splitting decreases from 129.7 to 127 kHz as temperature increases from 173 to 423 K, which can be translated to the amplitude of imidazolate linker rotation increasing from 21.8 to 26.9º as temperature increases as shown in the blue curve and Figure 2.11. Unlike ZIF-7, the temperature dependence of jump angle of linkers in ZIF-11 is composed of two regions. The rotational linker motion is more sensitive to temperature below 273 K. The T_1 relaxation of neat d-ZIFs will be discussed together with confined ZIFs in the next chapter.

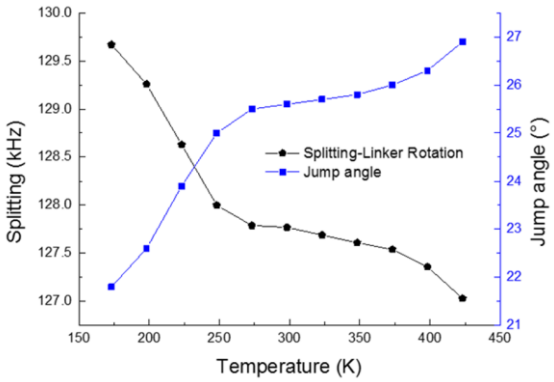

Figure 2.10: Pake splitting and jump angle of d-ZIF-11 measured from 173 to 423 K.

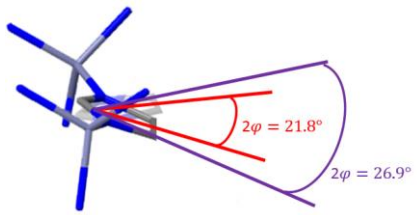

Figure 2.11: Temperature dependence of ZIF-11 linker jump angle at 173 K (red) and 423 K (purple).

2.5 Conclusion

By means of ^{2}H solid echo line shape analysis, linkers of these three ZIFs with different topology and imidazolate exhibit detectable mobility. As shown in Figure 2.12, all linker rotations within these ZIFs exhibit a positive temperature dependency while ZIF-8 is the most flexible ($\sigma_{ZIF\text{-}8} = \pm 18.9^{o}$ to $\pm 21.2^{o}$) and ZIF-7 ($\sigma_{ZIF\text{-}7} = \pm 10.7^{o}$ to $\pm 12.2^{o}$) is the most rigid by comparing their linker jump angles. The framework of ZIF-11 exhibits slightly flexible compare to that of ZIF-7 ($\sigma_{ZIF\text{-}11} = \pm 10.9^{o}$ to $\pm 13.5^{o}$).

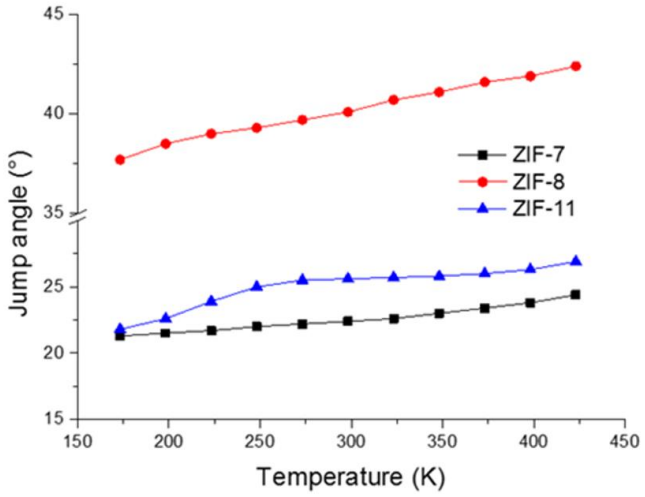

Figure 2.12: Jump angles of neat d-ZIFs.

CHAPTER 3. FABRICATION AND INVESTIGATION OF ISOTOPICALLY-ENRICHED ZIF-LOADED MMMS

3.1 Introduction

ZIF-loaded mixed matrix membranes are created to overcome fabrication issues of pure ZIF membranes and performance limitations of the polymer matrix; however, the interaction between two phases may play a crucial role in separation performance remains unclear. In this chapter, we directly investigate the polymer confinement effects on imidazolate linker rotations in ZIF-loaded mixed matrix membranes via solid-state NMR techniques and analysis.

Specifically, isotopically-enriched ZIF crystals discussed in Chapter 2 were incorporated into a Torlon® polymer matrix through standard mixed matrix membranes fabrication protocols. ^{2}H solid echo NMR line-shape analysis and T_1 saturation recovery experiments were performed to directly investigate the imidazolate linker rotations within the Torlon® polymer matrix confining the ZIF particles.

3.2 Fabrication Experiments

D-ZIF crystals were incorporated into mixed matrix membranes after all ^{2}H NMR experiments on neat d-ZIFs were completed. We hypothesize that a polymer with a large bulk modulus should change the dynamics of the ZIF material in an observable way. To test this hypothesis, Torlon® with a bulk modulus of 15 GPa, was selected as the polymer matrix for the NMR experiments on ZIF-loaded mixed matrix membranes. In addition, a

high crystal loading of about 30 wt% was chosen to significantly enhance the signal-to-noise ratio in the Pake patterns of the d-ZIF-loaded MMMs.

Powders of Torlon® 4000T-HV (Solvay) were dried at 110 ºC under dynamic vacuum for 24 hours. 50 mg of dried Torlon® powder was dissolved in 10 g N-Methyl-2-pyrrolidone solvent (BDH) in a 20 ml sample vial to form a dilute polymer solution (a so-called "prime dope"). At first, 270 mg isotopically-enriched ZIF crystals were dispersed evenly into the prime dope with the help of a sonication horn (Branson). After this dispersing step, the remaining 580 mg dried Torlon® 4000T-HV powder was added to the prime dope and mixed on a rolling mixer over 72 hours to fully dissolve the polymer.

The membrane dope was degassed overnight before casting to prevent non-selective holes formed via gas bubbles from evaporating solvent. A standard knife casting technique [33] was utilized to fabricate d-ZIF/Torlon® mixed matrix dense film in a clean glove bag purged with N_2 three times. After drying the wet membrane in the glove bag at 50 ºC over 72 hours, the as-fabricated d-ZIF-loaded MMMs were annealed at 200 ºC under dynamic vacuum for 24 hours.

3.3 Solid-state NMR experiments

3.3.1 Solid-State NMR Sample Preparation

Solid-State NMR samples were prepared by loading about 100 mg lab-fabricated d-ZIF-loaded mixed matrix membrane into a 5 mm (o.d.) and 30 mm (length) Norell® NMR tube. To fit the mixed matrix membrane nicely into the NMR tube, the d-ZIF-loaded MMM was cut into strips with 3 mm widths and 28 mm lengths and were packed neatly into the

tube. The two open ends of the tube were sealed with PTFE thread sealant tape. The sample was kept at 130 ºC under dynamic vacuum before the NMR testing.

3.3.2 Solid-State NMR Instrument Set-up

The experiments were performed on a wide-bore 7 Tesla Bruker AV3-HD 300 NMR spectrometer with 5mm probehead with a solenoid coil optimized for ^{2}H with Larmor frequency at $\frac{\omega_0}{2\pi} = 46$ MHz and wide-bore 9.4 Tesla Bruker AV3 400 NMR spectrometer with 5 mm probehead with a solenoid coil optimized for ^{2}H with Larmor frequency at $\frac{\omega_0}{2\pi} =$ 61 MHz.

^{2}H-solid echo experiments were carried out with pulse sequence of 90^o_x-τ_1-90^o_y-τ_2-acquisition-t. For ZIF-7 and ZIF-11 containing Torlon® mixed matrix membranes, the pulse length was set to be 4 µs and the delay between pulses was 30 µs, 1024 scans were recorded with a repetition delay of 10s (6144 scans for Torlon® confined ZIF-8). The number of scans was doubled due to the low intensity of deuterons in d-ZIF-loaded MMMs. Spectra were Fourier transformed starting with the data point of the echo maximum after an exponential multiplication leading to a line broadening of 3000 Hz.

Spin-lattice relaxation times (T_1) were obtained through saturation recovery experiments using the following pulse sequence: train of pulses-VD (Variable Decay)-acquisition-train of pulses-VD'-acquisition. VD_{MAX} is set at about 5 times of T_1 so the longitudinal magnetization is recovered completely before the next train of pulses, which FID gives the maximum signal each time. Experiments were carried through a broad temperature range, 173 to 423 K, controlled with a flow of nitrogen gas.

3.4 Results and Discussions

In this Chapter, ^{2}H solid echo NMR experiments were utilized to study the amplitude of imidazolate linker motion in d-ZIF-loaded mixed matrix membranes. We first tested d-ZIF-8/Torlon® mixed matrix membranes. All spectra of d-ZIF-8-loaded Torlon® MMMs measured at different temperatures are very similar to free standing d-ZIF-8, which indicates that Torlon® polymer confinement does not change this type of molecular motion of the imidazolate linkers within d-ZIF crystals. As discussed in previous Chapter, we can derive the amplitude of imidazolate linker rotation in d-ZIF-8 from either narrow or wide splittings in the Pake patterns. In addition, due to the relatively low signal intensity when d-ZIF-8 crystals loaded in Torlon® polymer matrix, we would focus on the splitting contributed from CD_3 in this Chapter.

Splittings and Jump angles of neat and confined d-ZIF-8 measured at different temperatures are summarized in Table 3.1. As shown in Figure 3.1, the rotation angle also showed similar temperature sensitivity to neat d-ZIF-8, which increased from 38.3 to 43.6º ($\sigma_{C\text{-}ZIF\text{-}8} = \pm$ 19.2 º to $\pm$ 21.8 º) with an increase in temperature from 173 to 423 K. Surprisingly, compared with neat d-ZIF-8, the amplitude of the linker rotation is slightly increased when placed in a Torlon® environment. However, the small difference is within experimental error. We can conclude that strong polymer confinement has negligible effect on the amplitude of imidazolate linker rotation within relative flexible ZIF-8 crystals.

Table 3.1: Splittings and Jump angle of neat and confined d-ZIF-8 at different temperatures.

	D-ZIF-8		D-ZIF-8/Torlon MMMs	
Temperature (K)	Splittings (kHz)	Jump angle (°)	Splittings (kHz)	Jump angle (°)
173	36.39	37.7	36.2	38.3
198	36.14	38.5		
223	35.98	39	35.9	39.3
248	35.91	39.3		
273	35.78	39.7	35.6	40.4
298	35.73	39.9		
323	35.46	40.7	35.2	41.5
348	35.34	41.1		
373	35.2	41.6	34.9	42.5
398	35.1	41.9		
423	34.94	42.4	34.6	43.6

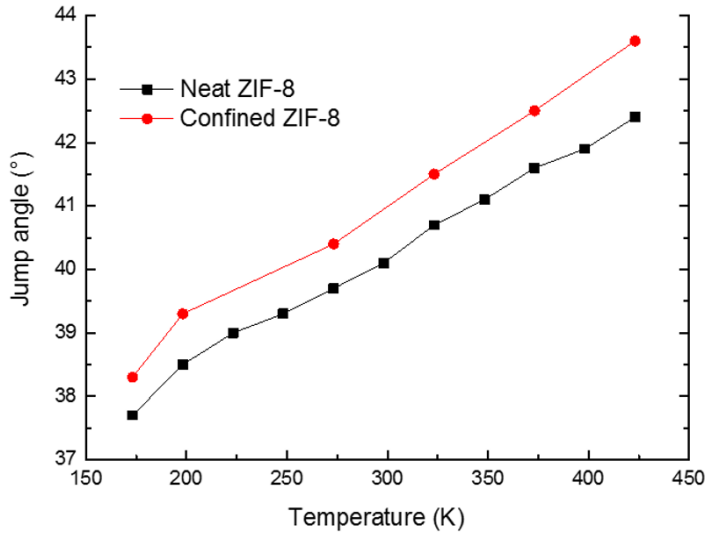

Figure 3.1: Jump angles of neat and confined d-ZIF-8s.

The amplitude of imidazolate linker rotation of d-ZIF-7 confined in Torlon® mixed matrix membranes were also studied through the same ^{2}H solid echo NMR experiments. Not surprisingly, all spectra of Torlon® matrix confined d-ZIF-7 measured at different temperatures are also almost identical to those of free standing d-ZIF-7, which implies the

same type of molecular motions with similar amplitude rotation angles of benzimidazole linkers in neat and confined d-ZIF-7.

Splittings and Jump angles of neat and confined d-ZIF-8 measured at different temperatures are summarized in Table 3.2. As shown in Figure 3.2, the amplitude of linker rotation in Torlon® matrix confined d-ZIF-7 increased from 20.9 to 23.8º ($\sigma_{C\text{-}ZIF\text{-}7} = \pm 10.5$ º to ± 11.9 º) as temperature increases from 173 to 423 K; while that in free standing d-ZIF-7 increased from 21.3 to 24.4º ($\sigma_{ZIF\text{-}7} = \pm 10.7$ º to ± 12.2 º). The small difference is within experimental error. We can conclude that strong polymer confinement also has negligible effect on the amplitude of imidazolate linker rotation within relative rigid d-ZIF-7 crystals.

Table 3.2: Splittings and Jump angle of neat and confined d-ZIF-7 at different temperatures.

	D-ZIF-7	D-ZIF-7/Torlon MMMs		
Temperature (K)	Splittings (kHz)	Jump angle (°)	Splittings (kHz)	Jump angle (°)
173	129.9	21.3	130.1	20.9
198	129.8	21.5	129.9	21.3
223	129.7	21.7	129.7	21.7
248	129.6	22	129.6	22
273	129.5	22.2	129.5	22.2
298	129.4	22.4	129.4	22.4
323	129.3	22.6	129.3	22.6
348	129.1	23	129.1	23
373	128.9	23.4	128.9	23.4
398	128.7	23.8	128.8	23.6
423	128.4	24.4	128.7	23.8

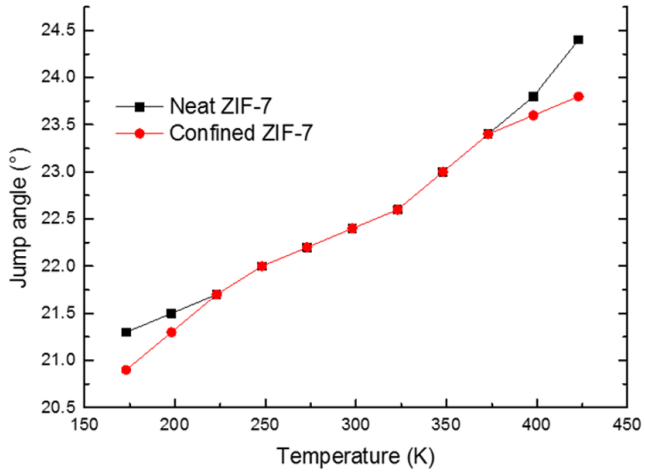

Figure 3.2: Jump angles of neat and confined d-ZIF-7s.

The same experiment was repeated on d-ZIF-11 confined in Torlon® mixed matrix membranes. Similar to other two ZIF crystals, all spectra of Torlon® matrix confined d-ZIF-11 measured at different temperatures are almost identical to those of free standing d-ZIF-11. Indeed, the same conclusion can be drawn regarding the type of molecular motions of benzimidazole linkers observed in neat and confined d-ZIF-11; i.e., they are identical.

Splittings and Jump angles of neat and confined d-ZIF-11 measured at different temperatures are summarized in Table 3.3. As shown in Figure 3.3, the amplitude of linker rotation in Torlon® matrix confined d-ZIF-11 increased from 21.4 to 27º ($\sigma_{C\text{-}ZIF\text{-}11} = \pm 10.7$ º to ± 13.5 º) as temperature increases from 173 to 423 K; while that in free standing d-ZIF-7 increased from 21.8 to 26.9º ($\sigma_{ZIF\text{-}11} = \pm 10.9$ º to ± 13.5 º). The small difference is within experimental error.

Table 3.3: Splittings and Jump angle of neat and confined d-ZIF-7 at different temperatures.

	D-ZIF-11		D-ZIF-11/Torlon MMMs	
Temperature (K)	Splittings (kHz)	Jump angle (°)	Splittings (kHz)	Jump angle (°)
173	129.67	21.8	129.9	21.4
198	129.26	22.6	129.3	22.6
223	128.63	23.9	128.9	23.4
248	128	25	128.3	24.5
273	127.79	25.5	127.6	25.8
298	127.77	25.6	127.5	26
323	127.69	25.7	127.4	26.2
348	127.61	25.8	127.3	26.4
373	127.54	26	127.2	26.6
398	127.36	26.3	127.1	26.8
423	127.03	26.9	126	27

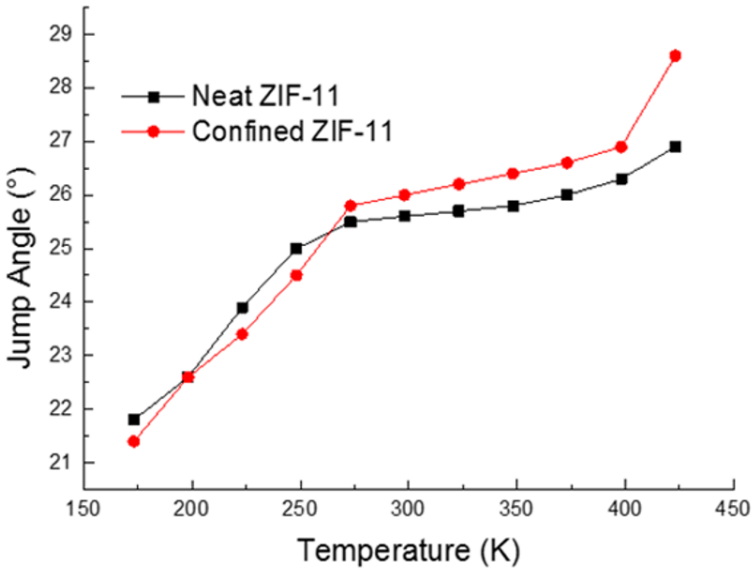

Figure 3.3: Jump angles of neat and confined d-ZIF-11s.

In this work, the polymer confinement effects on the amplitude of imidazolate linker rotation are directly studied in Torlon® matrix confined d-ZIF-7, d-ZIF-8, and d-ZIF-11. Surprisingly, the amplitudes of motions in these ZIFs are not influenced by strong polymer

compression induced by Torlon® matrix. We can conclude that the geometry of the linker motions was insensitive to polymer surroundings.

T_1 relaxation times can be utilized to calculate the activation energy of the imidazolate rotational motion. The T_1 relaxation times of neat and confined ZIFs are measured through saturation recovery method carried through a broad temperature range and controlled with a flow of nitrogen gas. T_1 relaxation times measured for d-ZIF-8 using a Bruker 300 shows interesting temperature dependence as shown in Figure 3.4. The resulting T_1 relaxations are a combination of both CD_3 fast self-rotation and the imidazolate linker rotation. T_1 relaxations of CD_3 is dominated by that of the fast local self-rotation [54], which is likely independent of the polymer confinement effect. As a result, T_1 relaxation for neat and confined d-ZIF-8 exhibit very similar temperature dependence. However, polymer confinement induced by Torlon® significantly reduced the time scale of T_1 relaxation by almost 50%, this result clearly indicates that the motion of linker rotation within ZIF-8 is affected by polymer confinement. Due to the noise from CD_3 fast local self-rotation, it is very challenging to obtain the frequency of imidazolate linker motions.

Due to the complexity of T_1 interpretation brought by the co-existing of two motions of 2-methylimidazole, we focus on d-ZIF-11 with imidazolate linkers that undergo solo rotational motion.

The Arrhenius plot of ^2H T_1 relaxation measured for d-ZIF-11 at Bruker 300 and 400 in a board ranges of temperature is as shown in Figure 3.5 and Figure 3.6 correspondingly.

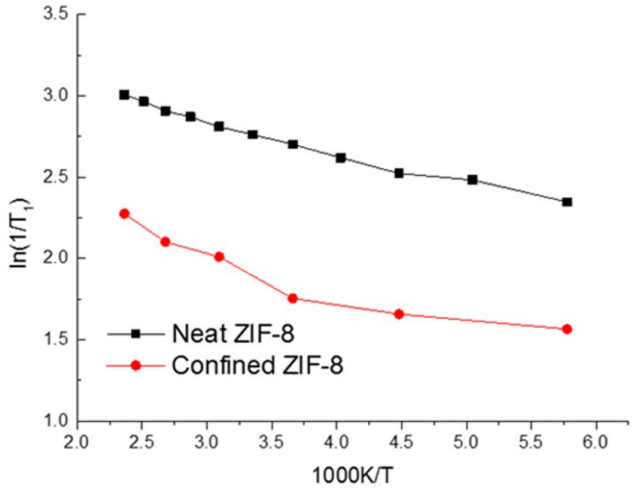

Figure 3.4: Arrhenius plot of ^2H T_1 relaxation rate at Bruker 300.

At 373 K, T_1 reaches a local minimum and goes to an ascending curve; while the local minimum of T_1 confined in Torlon® is found to be at 323 K as observed using a Bruker 300. This change directly shows that the frequency of imidazolate linker motion in neat d-ZIF-11 is slower compare to that in d-ZIF-11 confined in Torlon® matrix, which indicates that polymer confinement affects the linker motion. The experiment was repeated in Bruker 400, local minimum of T_1 are not observed since relaxation time scale is strongly dependent on the magnetic field of instruments. As shown in both figures, when temperature is below 323 K, relaxation of neat and confined d-ZIF-11 showed different temperature dependence.

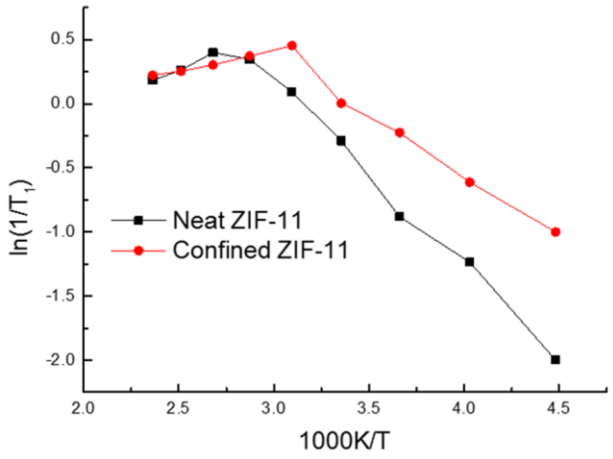

Figure 3.5: Arrhenius plot of ^2H T_1 relaxation rate at Bruker 300.

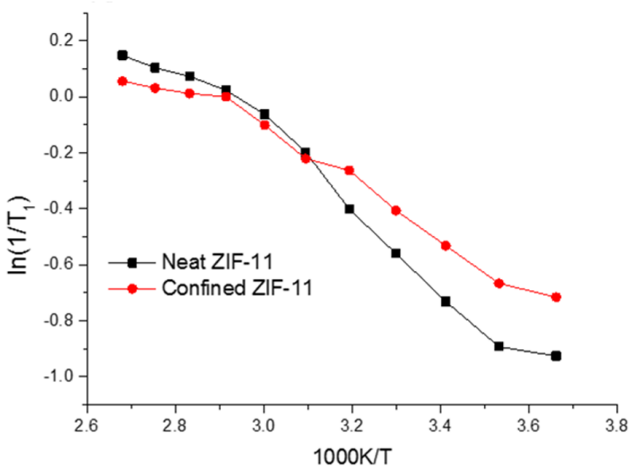

Figure 3.6: Arrhenius plot of ^2H T_1 relaxation rate at Bruker 400.

For a thermally activated process, the activation energy (E_A) is required to overcome the energy barrier separating the two mean equilibrium positions [60]. The activation energy can be obtained from an Arrhenius equation as function of temperature. In the extreme narrowing limit (which is molecular motion faster than MHz [42]), E_A is extracted from the slope of the Arrhenius plot of the temperature variation of log ($1/T_1$).

In this work, the activation energies of linker rotation are derived to be 12.3 kJ/mol and 8.4 kJ/mol in neat and confined d-ZIF-11 correspondingly. Due to the confinement effect from Torlon® matrix, the activation energy is lowered by 32%. Bruker 400 spectrometer showed similar results, with activation energy derived to be 12.9 kJ/mol and 8.8 kJ/mol in neat and confined d-ZIF-11. Polymer confining might be weakened due to different thermal expansion coefficients of Torlon® polymer matrix and d-ZIF-11; when temperatures are higher than 323 K, neat and confined d-ZIF-11 have very close T_1 relaxations.

3.5 Conclusion

^{2}H solid-echo line shape and ^{2}H spin-lattice relaxation analysis allows us to directly investigate the motion of imidazolate linkers in d-ZIF crystals. All three ZIFs have very mobile linkers; unlike other known MOFs (MOF-5, UIO-66, MIL-47), the amplitudes are small. d-ZIF-8 is the most flexible framework and has the largest linker rotation from $\pm$ 18.9º to $\pm$ 21.2º as temperature increases from 173 to 423 K, compared d-ZIF-7 from $\pm$ 10.7 º to $\pm$ 12.2 º, d-ZIF-11 from $\pm$ 10.9 º to $\pm$ 13.5 º over the same temperature range. The Torlon® polymer compressive effects on linker rotation are also studied. Surprisingly, the amplitudes of linker rotation are not influenced by polymer compression due to almost identical Pake pattern line shapes and very similar amplitudes of linker rotation linker rotation are obtained. Although the geometry of the linker motions was not affected by polymer confining, the ^{2}H spin-lattice relaxation of imidazolate linkers was found to be sensitive to the confinement effect. The activation energy of benzimidazole rotations in neat ZIF-11 is measured to be about 12.3 kJ/mol, while polymer compressive force lowered such energy by about 32%. A lower activation energy indicates that the energy barrier

separating the two mean equilibrium positions of imidazolate linkers is reduced due to the Torlon® confinement. As a result, the imidazolate linkers likely tend to flip more often under polymer confinement. We hypothesized that the increased frequency of imidazolate linker rotation would have more chances to bounce back molecules diffusing through the aperture, which would lower the diffusivity of guest molecules and enhance diffusive selectivity.

CHAPTER 4. GAS SORPTION AND PERMEATION IN ZIF-11/TORLON® MIXED MATRIX MEMBRANES

4.1 Introduction

In the early literature, the design of ZIF-loaded mixed matrix membranes was based on the assumption that transport and sorption properties of the dispersed ZIFs and surrounding polymer matrix are independent of the existence of each other. However, work mentioned in previous Chapters showed that although Torlon® polymer confining does not change the amplitude of imidazolate linker rotation in confined ZIFs, the activation energy of imidazolate linker rotation is significantly reduced.

In this Chapter, the gas sorption and permeation properties of the ZIF-11/Torlon® mixed matrix membranes were studied in an effort to establish a link between the microscopic and macroscopic properties of this system. To clearly elucidate such an effect, a series of neat ZIF-11 and confined ZIF-11s were systematically studied. As mentioned in previous Chapters, ZIF-11 with relatively moderate intrinsic flexibilities were used as the ZIF fillers in the ZIF-loaded MMMs. In addition, three polymers 6FDA-DAM, Matrimid® 5218, and Torlon® with different polymer bulk (compression) moduli will be utilized as the polymer matrix. In this Chapter, volumetric dosing and pressure decay system and isochoric permeation system were utilized to study the adsorption and transport propertied of as-fabricated ZIF-loaded MMMs.

4.2 Experiments

4.2.1 Preparation of shape and sized controlled ZIF crystals

ZIF-11 crystals used in this Chapter were prepared through modified solvothermal synthesis protocol discussed in previous Chapter. Crystals of controlled size and shape are required in this work. For instance, relatively large crystals are preferred to eliminate the boundary effect in PFG-NMR intra-diffusion measurements; while relatively small crystals are required to prepare defect free MMMs with a reasonable film thickness. Enormous efforts were made to modify the literature available synthesis protocol for ZIF-11 crystals.

ZIF-11 crystals approximately ~ 5μm in size were prepared through modified solvothermal synthesis protocol reported by He et al. [56]. About 600 mg (4.91 mmol) benzimidazole (Alfa Aesar) was added to a mixture solution of 16.74 g methanol (VWR) and 3.75 g 18% ammonium hydroxide solution. The adding of ammonium hydroxide was intended for deprotonating of organic ligands. About 549 mg (2.46 mmol) $Zn(O_2CCH_3)_2 \cdot 2H_2O$ (Alfa Aesar) was added to a mixture solution of 16.74 g methanol (VWR) and 12.99 g toluene (VWR). Toluene acts as the structure template in the cages of ZIF-11 which is crucial for the construction of such crystal. The later solution was added to former solution and stirred for 2 hours at room temperature. Reaction time should be precisely controlled to avoid the formation of larger crystals. The product of ZIF-11 were recovered by vacuum filtration and centrifugation, followed by extensive washing with methanol. The product was activated at 130 at dynamic vacuum for 24 hours.

As shown in Figure 4.1, monodispersed uniformed size and shape controlled ZIF-11 crystals were ultimately achieved.

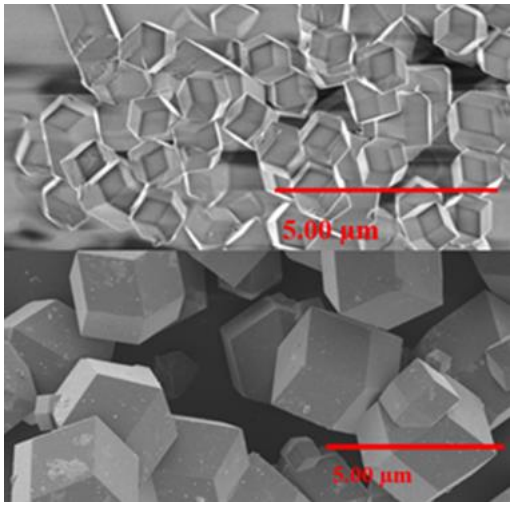

Figure 4.1: SEM images of size and shape controlled ZIF-11.

4.2.2 Preparation of high molecular weight polymers

High molecular weight polymers with different bulk moduli used in this Chapter were either commercially available or lab synthesized. Matrimid® 5218 (~3 GPa) was purchased from Huntsman and Torlon® 4000T-HV (~ 15 GPa) was kindly supplied by Solvay. In addition, high molecular weight 6FDA-DAM (~1 GPa) was fabricated via the lab synthesis as shown in Figure 4.2.

Both 6FDA (dianhydrides, 4,4'-(Hexafluoroisopropylidene)diphthalic anhydride) (BTC) and DAM (diamine diaminomesitylene) (Sigma Aldrich) were dried under dynamic vacuum at room temperature before purification. Monomers were purified in sublimation apparatus at 215 °C (6FDA) and 100 °C (DAM) under 100 mTorr. The equimolar sublimated monomers were stored under dynamic vacuum. The exposure of 6FDA in the air may will react with moisture, while stochiometric ratio is crucial in this reaction. Separately, NMP (N-Methyl-2-pyrrolidone) (VWR) and acetic anhydride (Sigma Aldrich)

solvents were dried using activated molecular sieves 3A. Reactors were purged with N_2 and propane torched under purging before formation of the polyamic acid.

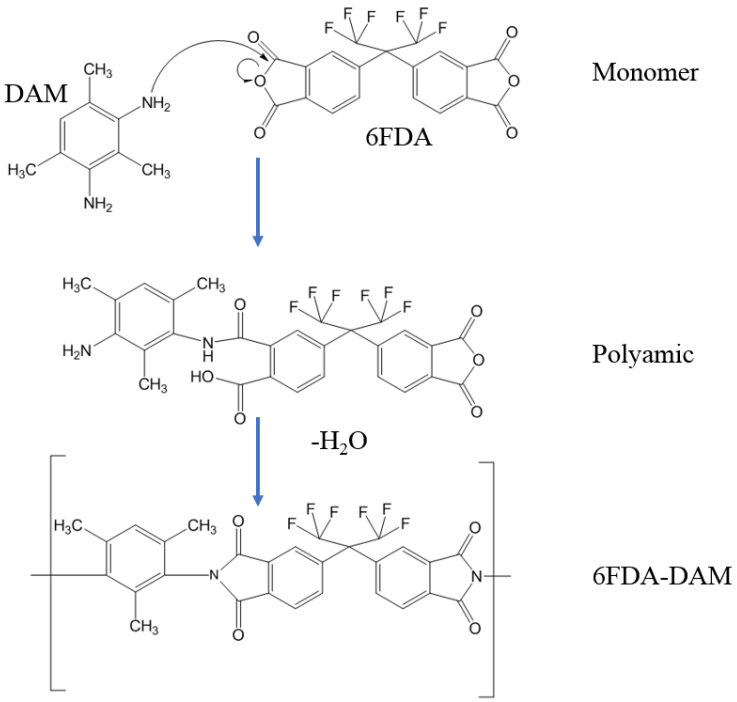

Figure 4.2: Formation of 6FDA-DAM.

Sublimated DAM monomer was dissolved into NMP under stirring and purging cooled within ice-water bath. 6FDA monomer was added into former solution in four times. Beta-picoline was added to start the chemical imidazation 24 hours after the significant rise of solution viscosity. The mass ratio of beta-picoline and acid anhydride is 1:10. Acetic anhydride was added when the beta-picoline is completely dissolved. The solution was under N_2 purging at room temperature for 24 hours. The product is precipitated in methanol solution, followed by extensive washing with methanol. The product is dried under dynamic vacuum at 200 °C for 24 hours.

4.2.3 Preparation of pressure decay cell and isochoric permeation system measurements

Unlike the high loading of d-ZIF-loaded MMMs studied in previous Chapter, the ZIF crystals loading of MMMs in this Chapter is about 10%. The fabrication process of these membranes was discussed in the previous Chapter.

To prepare the pressure decay cell sample, as-made membranes were cut into ½" wide and 3" long strips. These membrane strips were heavily packed together and neatly rolled into a column that fits into the sample container (a ½" VCR male housing) of the cell. The temperature of the experiment was set to 35 °C, which was controlled by an oil bath. The isotherms of CO_2, CH_4, and N_2 for the as-made pure polymer membranes, ZIF-loaded MMMs, and neat ZIF crystals were measured.

To prepare the isochoric permeation system sample, as-made defect-free membrane was cut into a 1" diameter circle. Before attaching that circle membrane into a mask, the membrane thickness was measured 20 times through peacock dial thickness gauge. The area of the membrane was measure through ImageJ after experiment. The temperature of the experiment was set to 35 °C controlled by heating fan in a permeation box. The permeabilities of CO_2, CH_4, N_2 through the as-made pure polymer membranes and ZIF-loaded MMMs were measured.

4.3 Sorption Experiment Results and Discussion

In this Chapter, volumetric dosing and pressure decay technique was utilized to study the gas adsorption in ZIF-loaded mixed matrix membranes. We first measured the CO_2, CH_4, N_2 sorption isotherms of ZIF-11 at 35 °C and plotted in Figure 4.3. Due to the

relatively rigid structure of ZIF-11, sorption of CO_2 and CH_4 increase as the pressure goes up, while a "plateau" is observed at higher pressure characteristic of a Langmuir isotherm. Using the Langmuir model [61], the saturation capacity for CO_2 and CH_4 are estimated to be 0.988 mmol/g and 0.328 mmol/g, and the affinity constants are 0.0199 1/psi and 0.0156 1/psi, respectively. Due to the small window size of ZIF-11, N_2 was hardly adsorbed at all as shown in the red curve in Figure 4.3.

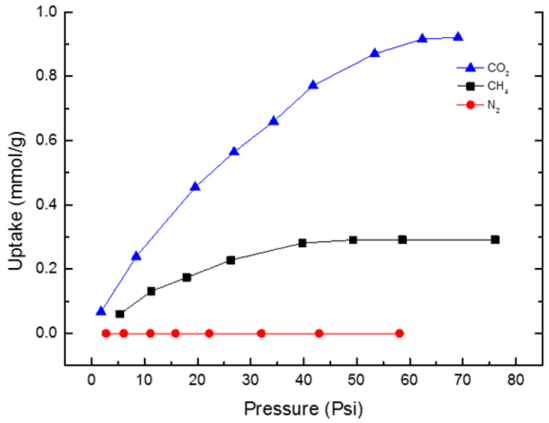

Figure 4.3: Gas uptake of ZIF-11 crystals at 35 °C.

We measured the gas uptake of pure Torlon®, Matrimid®, and 6FDA-DAM polymer membranes at 35 °C, which were then compared with the isotherms of ZIF-11-loaded MMMs. Pure Torlon® membrane with thickness of ~25.6 μm showed negligible N_2 and CH_4 uptakes and slow diffusion rate under 80 psi, which may not actually demonstrate the effect on sorption properties induced by filler-matrix interaction. Since pure ZIF-11 crystals also showed almost no N_2 uptake, we subsequently focused on CO_2 and CH_4 uptakes in ZIF-11/Matrimid® and ZIF-11/6FDA-DAM MMMs.

Sorption in glassy polymer can be described by the dual model accounting for sorption in the densified region described by the Henry's law and free volume described

by the Langmuir model. The Henry adsorption constant, saturation capacity, and affinity constant of CO_2 and CH_4 isotherms of tested membranes at 35 °C are listed in Appendix A.

Both CO_2 and CH_4 isotherms of pure Matrimid® membrane, free-standing ZIF-11 crystals, and ZIF-11/Matrimid® MMM were tested in pressure decay cell at 35 °C and plotted in Figure 22. The black curve and red curve showed the CO_2 isotherms of pure Matrimid® membrane and free-standing ZIF-11 crystals. The blue curve is the isotherm of simulated 10% ZIF-11/Matrimid® MMM, which contains contributions from the 10% sorption into the ZIF-11 crystals and 90% sorption into the pure Matrimid® membrane. A weighted average combination of these two isotherms will be obtained if there is no change in the sorption coefficient of either material once formulated into a composite. The pink curve is the isotherm directly measured for 10% ZIF-11/Matrimid® MMM; no difference is observed between the experimental and predicted isotherms.

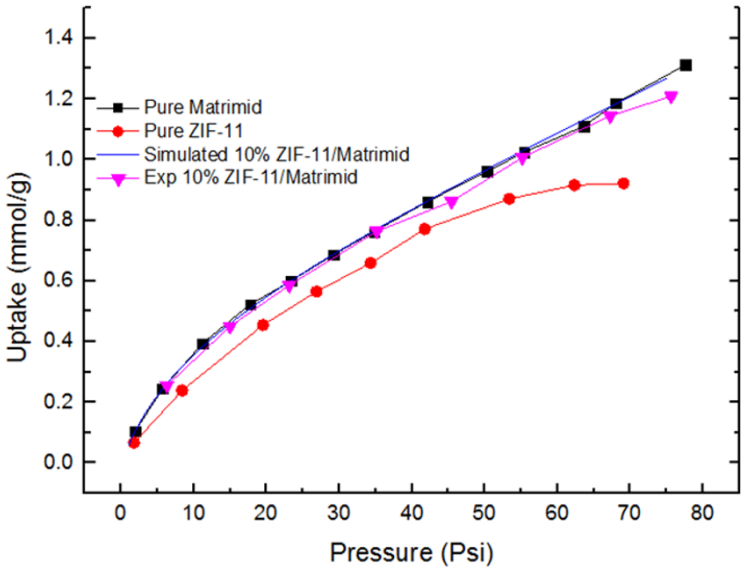

Figure 4.4: CO_2 uptake in ZIF-11/Matrimid® MMMs.

The same series of experiments was repeated on ZIF-11-loaded 6FDA-DAM MMM. As shown in Figure 4.5, notable differences between the predicted and experimental MMM isotherms were observed, suggesting that one of the materials may exhibit a change in sorptivity after formulation into a composite. Additional and more accurate measurements are needed to confirm this finding.

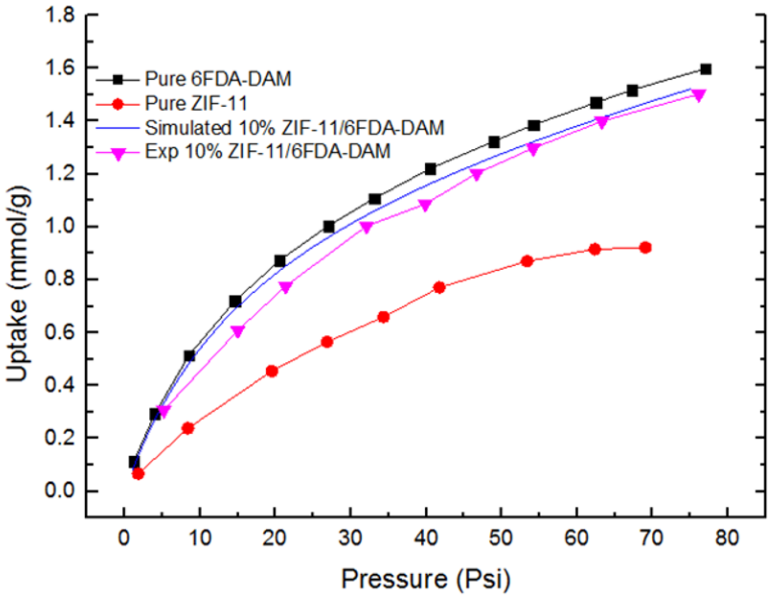

Figure 4.5: CO_2 uptake in ZIF-11/6FDA-DAM MMMs.

In addition to CO_2 isotherms, we also studied CH_4 isotherms for ZIF-11-loaded MMMs as plotted in Figure 4.6 and Figure 4.7. Similar to the case of CO_2, there is essentially no difference in the predicted and experimental MMM isotherms for the Matrimid® case, but there are small but notable deviations between these two isotherms for the 6FDA-DAM polymer matrix. The small reduction in CO_2 and CH_4 isotherms may be a result of small unit cell contractions within the ZIF-11 crystal as a result of confinement in a polymer matrix. However, probing this hypothesis requires the use of synchrotron x-ray facilities, which were not available over the course of this work.

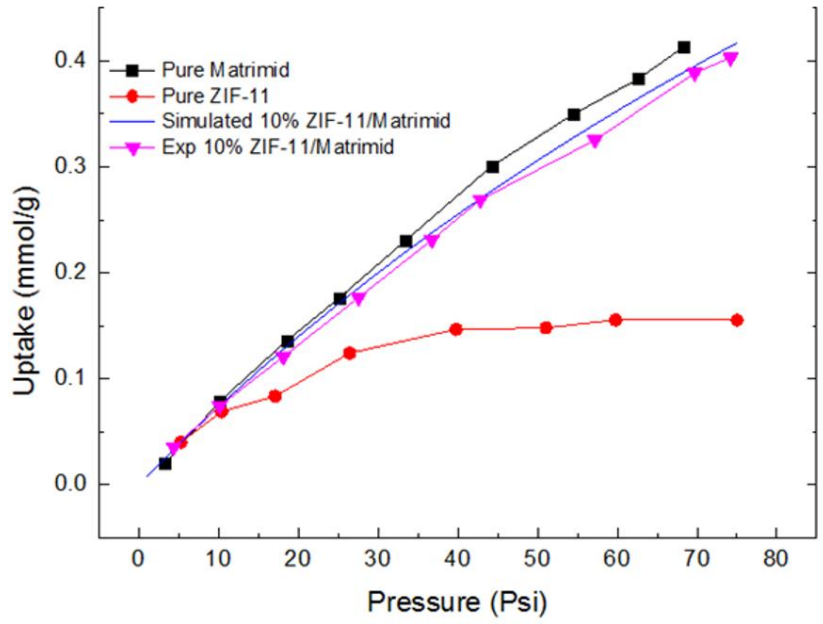

Figure 4.6: CH_4 uptake in ZIF-11/Matrimid® MMMs.

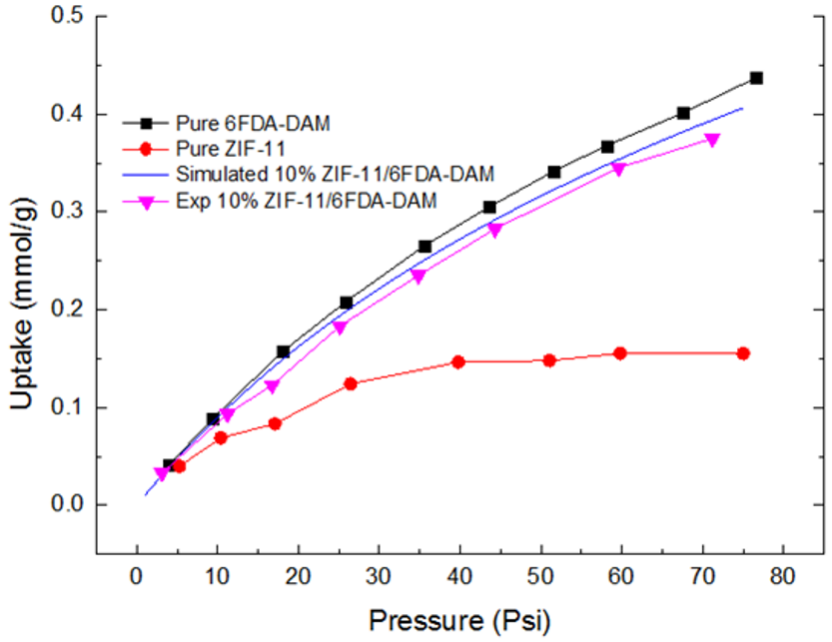

Figure 4.7: CH_4 uptake in ZIF-11/6FDA-DAM MMMs.

4.4 Permeation Experiment Results and Discussion

In this Chapter, author-made isochoric gas permeation systems were utilized to study the gas (N_2, CH_4, CO_2) permeation in pure polymer and ZIF-11-loaded mixed matrix membranes at 35 °C. Membrane thicknesses and areas are listed in Appendix B.

The CO_2 and N_2 permeation results are shown in Figure 4.8. As compared to the pure Matrimid®, Torlon®, and 6FDA-DAM polymer membranes, the CO_2 permeabilities of 10% ZIF-11-loaded mixed matrix membranes increased by 26.6%, 18.8%, and 30.0% respectively; while the N_2 permeabilities of ZIF-11-loaded mixed matrix membranes only increased by 9.5%, 8.0%, and 20.0%. As a result, the ideal selectivities of CO_2/N_2 were enhanced.

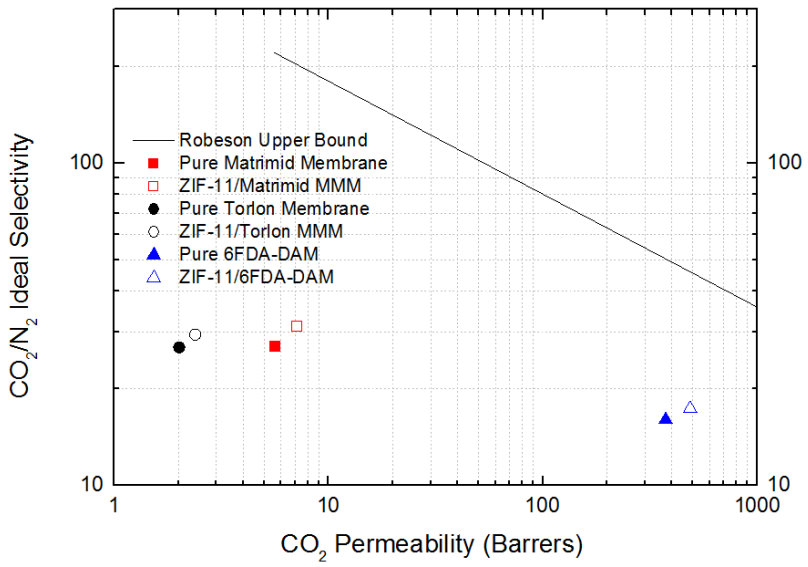

Figure 4.8: CO_2/N_2 separation performance of ZIF-11/MMMs.

The CH_4 and CO_2 permeation results are shown in Figure 4.8. Similar to N_2, the permeabilities of CH_4 through ZIF-11-loaded mixed matrix membranes increased less than CO_2. As a result, the ideal selectivities of CO_2/CH_4 enhanced.

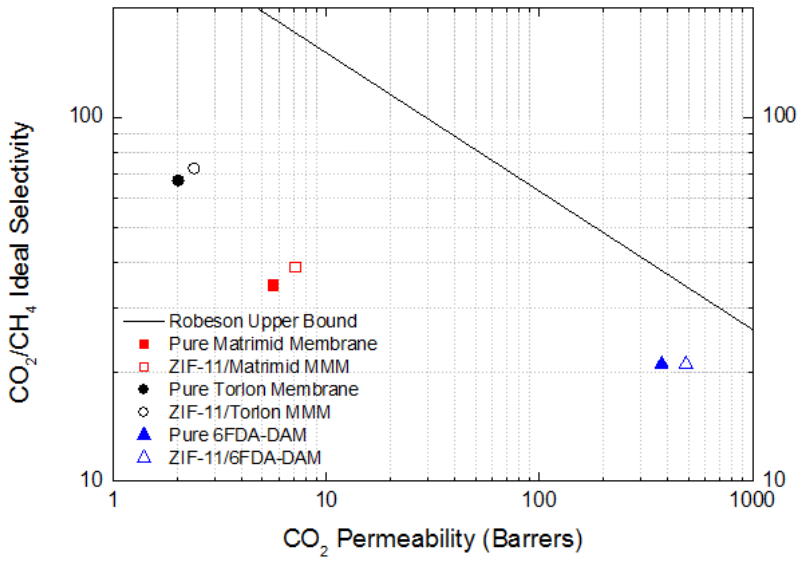

Figure 4.9: CO_2/CH_4 separation performance of ZIF-11/MMMs.

The permeability of CO_2 and CH_4 in the pure ZIF-11 crystals confined in mixed matrix membranes was back-calculated using permeabilities of pure polymer membranes and ZIF-11-loaded MMMs with 12.8 vol% loading using the Maxwell model (Equation 1.5, Section 1.2.2) [29]; the result are shown in Table 4.1.

The adsorption coefficient S (mmol/(g*Psi)) of CO_2 and CH_4 in dispersed ZIF-11 particles can be obtained in equation 1.3 $S = \frac{C_2 - C_1}{p_2 - p_1}$. Where C_1 (mmol/g) and C_2, p_1 (Psi) and p_2 are adsorbate concentrations and adsorbate pressure in the ZIF-11 fillers at the downstream side and upstream side of the membrane.

The transport diffusion coefficient D (m^2/s) of CO_2 and CH_4 in dispersed ZIF-11 particles can be obtained by equation 1.2, and the results are shown in as shown Table 4.1.

Table 4.1. Transport properties in the pure ZIF-11 phase in MMMs.

Matrix Polymer Supporting ZIF-11	P_{CH4}	P_{CO2}	S_{CH4}	S_{CO2}	D_{CH4}	D_{CO2}
	Barrer		mmol/(g*Psi)		$10^{-14}m^2/s$	
Matrimid®	0.378	35.011	0.00236	0.00802	35.1	955.8
Torlon®	0.0603	7.162	0.00241	0.0077	5.5	203.4
6FDA-DAM	149.337	3130.86	0.00238	0.00789	13759.7	86856.8

Comparing our transport results from those of our collaborators (Prof. Sergey Vasenkov, University of Florida), the intracrystalline diffusivities of CO_2 and CH_4 within pure ZIF-11 crystals obtained from PFG NMR at 308 K 5 Bar, are in the range of 2 $*10^{-10}m^2/s$ and 1 $*10^{-10}$ m^2/s, polymer confined ZIF-11 shows significantly reduced gas diffusivity. This finding supports the hypothesis that imidazolate linker tends to flip more often under polymer confinement effect probed solid-state NMR. In addition, the predicted permeability of CO_2 and CH_4 of ZIF-11 was calculated by the product of sorption coefficients obtained from isotherms and corrected diffusion coefficients from PFG-NMR as shown in table 4.2 and Figure 4.10. The predicted selectivity of CO_2/CH_4 though ZIF-11 were significantly enhanced when incorporated in Matrimid® and 6FDA-DAM polymer matrix.

Table 4.2. Predicted CO_2 and CH_4 permeabilities of ZIF-11.

Matrix Polymer Supporting ZIF-11	D_{CH4}	D_{CO2}	S_{CH4}	S_{CO2}	P_{CH4}	P_{CO2}	$\alpha_{CO2/CH4}$
	$10^{-10}m^2/s$		mmol/(g*Psi)		Barrer		
Matrimid®	0.96	2.3	0.00036	0.00570	18.4	845.5	46.0
6FDA-DAM			0.00034	0.00554	17.6	872.1	49.6
Free Standing			0.00240	0.00805	105.3	845.9	8.0

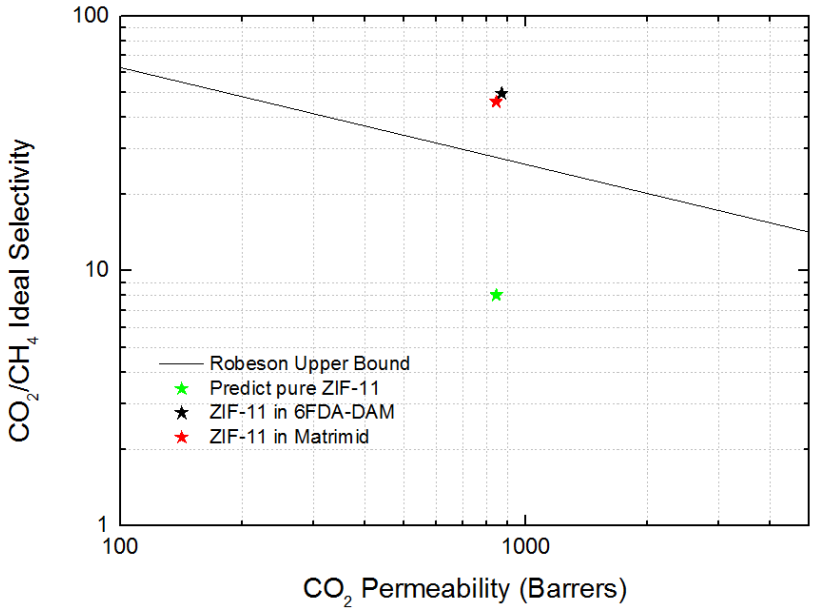

Figure 4.10: Predicted CO_2/CH_4 separation performance of ZIF-11s.

4.5 Conclusions

In this Chapter, polymer confining effects on adsorption and permeation properties of ZIF-loaded MMMs were studied. Size and shaped controlled ZIF-11 crystals were incorporated into a series of polymer matrixes (Matrimid®, Torlon®, and 6FDA-DAM). Volumetric dosing and pressure decay system and isochoric permeation system were applied in this work.

By comparing the CO_2 and CH_4 isotherms of simulated and experimental measured isotherms, a smaller uptake was observed in the case of Matrimid® and 6FDA-DAM. The lower isotherms can be explained by smaller physisorption in the polymer-crystal

contacting zone or through slight unit cell contractions as a result of compression by the polymer matrix.

The incorporation of ZIF-11 crystals into polymer matrix significantly increased the permeability and ideal selectivity of the membranes studied here. Transport diffusion coefficients of CO_2 and CH_4 in polymer confined ZIF-11 are obtained from permeation and sorption experiments, which are smaller than that of intracrystalline diffusivities of pure ZIF-11 obtained from PFG NMR by our collaborators. This finding directly supports our hypothesis of imidazolate linker tends to flip more often under polymer confinement probed by solid-state NMR. In addition, compare to free standing ZIF-11, ideal selectivity of CO_2 and CH_4 are enhanced due to the polymer confinement.

CHAPTER 5. CONCLUSION AND FUTURE WORK

5.1 Conclusion

Significant work is being devoted to the reduction of global energy consumption associated with industrial separations, with increasing attention being focused on membrane technology. In particular, mixed matrix membranes containing zeolitic imidazolate frameworks are an attractive alternative to conventional thermal separation processes and have received continuous attention from both academia and industry in the past years. However, as mentioned in Chapter 1, the interaction between the ZIF fillers and polymer matrix remains unclear. The overarching goal of this work was to understand the interplay between ZIF discrete phase and polymer matrix continues phase.

Chapter 2 of this work probed the imidazolate linker motion of ZIF crystals by utilizing solid-state NMR techniques. First of all, isotopically-enriched d-ZIF-7, d-ZIF-8, and d-ZIF-11 crystals were synthesized by modified solvothermal synthesis protocol. By means of ^{2}H solid echo line shape analysis and spin-lattice relaxation analysis, imidazolate linker rotations in free-standing ZIFs and polymer matrix confined ZIFs were studied. All three d-ZIFs have very mobile linkers with limited amplitudes of linker motion, but with limited amplitude of rotation. For all free-standing d-ZIF crystals, a positive temperature dependency was consistently observed. In addition, d-ZIF-8 was the most flexible structure i.e., it exhibited the largest amplitude of linker rotation; meanwhile d-ZIF-7 was the most rigid structure studied and displayed the smallest amplitude of the rotational motion.

Chapter 3 of this work directly probed how polymer confinement affects the imidazolate linker rotation using the same NMR experiments utilized in Chapter 2. For those d-ZIFs incorporated in Torlon®, Matrimid®, and 6FDA-DAM polymer matrix, the imidazolate linker motion still showed a positive temperature sensitivity; however, polymer confinement effects do not change the amplitude of this rotation. Surprisingly, the polymer compressive force lowered the activation energy of benzimidazole rotations in d-ZIF-11 by about 32%, which indicate the imidazolate linker flips more often in a polymer confined environment.

Chapter 4 of this work demonstrated the polymer confining effects on transport properties of ZIF-loaded MMMs through volumetric dosing and pressure decay system and isochoric permeation system. By comparing the linearly simulated isotherm of CO_2 and CH_4 isotherms and experimental isotherms, ZIF-11-loaded MMMs did not adsorb as much sorbate as expected. Reduction in the sorption coefficient could be a result of polymer rigidification around the ZIF crystal, or a slight reduction of in ZIF crystal unit cell volume as a result of compression from the polymer matrix. In addition, transport diffusion coefficients of CO_2 and CH_4 in polymer confined ZIF-11 are smaller than that of intracrystalline diffusivities of pure ZIF-11. This finding directly supports our hypothesis of imidazolate linker tends to flip more often under polymer confinement probed by solid-state NMR. In addition, compare to free standing ZIF-11, ideal selectivity of CO_2 and CH_4 are enhanced due to the polymer confinement.

The present work is the first example of studying polymer confining effects on imidazolate linker motion in ZIF crystals which will help develop ZIF-loaded MMMs with

tailored separation performance by engineering the interplay between ZIF crystals fillers and the polymer matrix.

5.2 Future work

The future work of this thesis are extensions of several parts. The first part should be further interpretation of spin-lattice relaxation analysis experiment. In this thesis, activation energy of imidazolate linker rotations were derived from an Arrhenius plot of T_1 relaxation time as a function of temperature. With the help of Bloembergen-Purcell-Pound (BPP) theory discussed in the first Chapter and spectral density analysis, the frequency in imidazolate linker rotation in the range of MHz can be estimated. By comparing the frequency of imidazolate linker rotation in neat and polymer confined ZIF crystals, the guest molecular diffusion coefficients can be potentially calculated using molecular modeling approaches.

In addition, to further study the polymer confinement effect to polymer itself, polymer matrix can be isotopically enriched by lab synthesizing through deuterated monomers. To eliminate the effect of porous fillers in analyzing the transport properties, non-porous materials can be incorporated into isotopically enriched polymer matrix. Moreover, the dynamics and changes in dynamics upon formation of the MMM of the polymer matrix can be studied using this approach.

In Chapter 4 of this work, 10 wt% ZIF-11 crystals were incorporated into polymer matrix. The polymer confinement effects of such small loading are relatively inobvious. To clearly demonstrate the polymer confinement effects on physisorption and transport properties of ZIF-loaded MMMs, higher ZIF crystals loading are recommended. In

addition, ZIF crystals with smaller size are recommended due to the relatively large external surface area of small crystals.

APPENDIX A

Table A1. Dual mode model.

Membrane	Gas	Henry Adsorption Constant	Saturation Capacity	Affinity Constant
		mmol/(g*Psi)	mmol/g	1/Psi
ZIF-11	CH_4	8.15	0.209	0.0476
Matrimid®		0	1.69	0.0047
ZIF-11/Matrimid®		0.0013	0.902	0.0067
Simulated		4.96	1.27	0.0057
6FDA-DAM		0.00131	0.627	0.015
ZIF-11/6FDA-DAM		0	0.919	0.0099
Simulated		0.0012	0.6	0.0149
ZIF-11	CO_2	2.22	1.62	0.0206
Matrimid®		0.0115	0.447	0.1251
ZIF-11/Matrimid®		0.01	0.535	0.087
Simulated		0.0113	0.473	0.1071
6FDA-DAM		0.00662	1.33	0.0615
ZIF-11/6FDA-DAM		0.00642	1.33	0.0444
Simulated		0.00623	1.29	0.0586

APPENDIX B

Table B1. Membrane thickness and area.

		Membrane Thickness (μm)	Membrane Area (cm^2)
Matrimid®	Mask 1	29.7	1.995
	Mask 2	28.1	2.134
ZIF-11/Matrimid®	Mask 1	32.4	2.228
	Mask 2	35.1	1.887
Torlon®	Mask 1	48.1	2.498
	Mask 2	47.6	2.476
ZIF-11/Torlon®	Mask 1	50.1	2.154
	Mask 2	47.3	2.669
6FDA/DAM	Mask 1	59.3	2.663
	Mask 2	58.7	2.657
ZIF-11/6FDA-DAM	Mask 1	57.2	2.417
	Mask 2	61.4	1.995

REFERENCES

[1] Eldridge, R. Bruce., Ind. Eng. Chem. Res. 32, 2208 (1993).

[2] Jarvelin, H. and Fair, J.R., Ind. Eng. Chem. Res. 32, 2201 (1993).

[3] Pimentel, Brian. R., Parulkar, Aamena., Zhou, Er-kang., Brunelli, Nicholas. A. and Lively, Ryan. P., CHEMSUSCHEM. 7, 3202 (2014).

[4] Park, Kyo. Sung., Ni, Zheng., Cote, Adrien. P., Choi, Jae. Yong., Huang, Rudan., Uribe-Romo, Fernando. J., Chae, Hee. K., O'Keeffe, Michael. And Yaghi, Omar. M., PNAS. 103, 10186 (2006).

[5] Bux, Helge., Liang, Fengyi., Li, Yanshuo., Carvillon, Janosch., Wiebcke, Michael. and Caro, Jurgen., J. Am. Chem. Soc. 131, 16000 (2009).

[6] Xie, Zhong., Yang, Jianhua., Wang, Jinqu., Bai, Ju., Yin, Huimin., Yuan, Bing., Lu, Jinming., Zhang, Yan., Zhou, Liang and Duan, Chunying., Chem. Commun. 48, 5977 (2012).

[7] Bux, Helge., Feldhoff, Armin., Cravillon, Janosch., Wiebcke, Michael., Li, Yan-Shuo. and Caro, Juergen., Chem. Mater. 23, 2262 (2011).

[8] Kang, Chao-Hsiang., Lin, Yi-Feng., Huang, Yao-Sheng., Tung, Kuo-Lun., Chang, Kai-Shiun., Chen, Jung-Tsai., Hung, Wei-Song., Lee, Kueir-Rarn. and Lai, Juin-Yih., J. Membr. Sci. 438, 105 (2013).

[9] Xu, Gengsheng., Yao, Jianfeng., Wang, Kun., He, Li., Webley, Paul. A., Chen, Chu-sheng. and Wang, Huanting., J. Membr. Sci. 385-386, 187 (2011).

[10] Li, Yan-Shuo., Bux, Helge., Feldhoff, Armin., Li, Guo-Ling., Yang, Wei-Shen. and Caro, Jurgen., Adv. Mater. 22, 3322 (2010).

[11] Bux, Helge., Chmelik, Christian., Krishna, Rajamani. and Caro, Juergen., J. Membr. Sci. 369, 284 (2011).

[12] Zhang, Xiongfu., Liu, Yaguang., Kong, Lingyin., Liu, Haiou., Qiu, Jieshan., Han, Wei., Weng, Lu-Tao., Yeung, King. Lun. and Zhu, Weidong., J. Mater. Chem. A. 1, 10635 (2013).

[13] Dong, Xueliang., Huang, Kang., Liu, Sainan., Ren, Rufei., Jin, Wanqin and Lin, Y.S., J. Mater. Chem. 22, 19222 (2012).

[14] Robeson, Lloyd. M., J. Membr. Sci. 320, 390 (2008).

[15] Freeman, Benny. D., Macromolecules. 32, 375 (1999).

[16] Koros, William. J. and Lively, Ryan. P., AIChE J. 58, 2624 (2012).

[17] Barrer, R.M. and James, S.D., J. Phys. Chem. 64, 417 (1960).

[18] Barrer, R.M. and James, S.D., J. Phys. Chem. 64, 421 (1960).

[19] Thompson, Joshua. A., Chapman, Karena. W., Koros, William. J., Jones, Christopher. W. and Nair, Sankar., Microporous Mesoporous Mater. 158, 292 (2012).

[20] Base, Subhankar., Cano-Odena, Angels. and Vankelecom, Ivo. F.J., Sep. Purif. Technol. 81, 31 (2011).

[21] Dai, Ying., Johnson, J.R., Karvan, Oguz., Sholl, David. S. and Koros, W.J., J. Membr. Sci. 401-402, 76 (2012).

[22] Bai, Yunxiang., Dong, Liangliang., Zhang, Chunfang., Gu, Jin., Sun, Yuping., Zhang, Lin. and Chen, Huanlin., Sep. Sci. Technol. 48, 2531 (2013).

[23] Liu, Xin-Lei., Li, Yan-Shuo., Zhu, Guang-Qi., Ban, Yu-Jie., Xu, Long-Ya. and Yang, Wei-Shen., Angew. Chem. Int. Ed. 50, 10636 (2011).

[24] Yang, Tingxu., Xiao, Youchang. and Chung, Tai-Shung., Energy. Environ. Sci. 4, 4171 (2011).

[25] Diaz, Kenya., Lopez-Gonzalez, Mar., Castillo, Luis. F. del. and Riande, Evaristo., J. Membr. Sci. 383, 206 (2011).

[26] Zhang, Chen. and Koros, William. J., J. Phys. Chem. Lett. 6, 3841 (2015).

[27] Buonomenna, M.G. and Golemme, G., *Advanced Materials for Membrane separation*, Bentham Science Publishers, 2012.

[28] Koros, W.J. and Fleming, G.K., J. Membr. Sci. 83, 1 (1993).

[29] She, S., PhD Dissertation, Georgia Institute of Technology, 2007.

[30] Zhang, Chen., Dai, Ying., Johnson, Justin. R., Karvan, Oguz. and Koros, William. J., J. Membr. Sci. 389, 34 (2012).

[31] Perez, Edson. V., Balkus Jr., Kenneth J., Ferraris, John. P. and Musselman, Inga. H., J. Membr. Sci. 328, 165 (2009).

[32] Zheng, Bin., Pan, Yichang., Lai, Zhiping. and Huang, Kuo-Wei., Langmuir. 29,

8865 (2013).

[33] Watanabe, Taku. and Sholl, David. S., Langmuir. 28, 14114 (2012).

[34] Zhang, Ke., Lively, Ryan. P., Zhang, Chen., Chance, Ronald. R., Koros, William. J., Sholl, David. S. and Nair, Sankar., J. Phys. Chem. Lett. 4, 3618 (2013).

[35] Verploegh, Ross. J., Nair, Sankar. and Sholl, David. S., J. Am. Chem. Soc. 137, 15760 (2015).

[36] Diestel, Lisa., Wang, Nanyi., Schwiedland, Barbel., Steinbach, Frank., Giese, Ulrich. and Caro, Jurgen., J. Membrane Sci. 492, 181 (2015).
[37] Mueller, Robert., Zhang, Suihua., Zhang, Chen., Lively, Ryan. and Vasenkov, Sergey., J. Membrane Sci. 477, 123 (2015).

[38] Sheng, Luqian., Wang, Chongqing., Yang, Fan., Xiang, Long., Huang, Xiaojian., Yu, Jian., Zhang, Lixiong., Pan, Yichang. and Li, Yanshuo., Chem. Comm. 53, 7760 (2017).

[39] Colin, A. Fyfe., Thomas, John. M., Klinowski, Jacek. and Gobbi, Gian. C., Angew. Chem. Int. Ed. 22, 259 (1983).

[40] Duer, M.J., *Introduction to Solid-State NMR Spectroscopy*, Blackwell Science Publishers, 2004.

[41] Fitzgerald, J.J., *Solid-State NMR Spectroscopy of Inorganic Materials*, American Chemical Society, 1999.

[42] Schmidt-Rohr, K. and Spiess, H.W., *Multidimentional Solid-State NMR and Polymers*, Academic Press, 1994.

[43] Antonijevic, Sara. and Wimperis, Stephen., J. Magn. Reson. 164, 343 (2003).

[44] Mizuno, Motohiro., Itakura, Naohisa. and Endo, Kazunaka., Chem. Phys. Lett. 416, 358 (2005).

[45] Gould, Stephanie. L., Tranchemontagne, David., Yaghi, Omar. M. and Garcia-Garibay, A., J. Am. Chem. Soc. 130, 3246 (2008).

[46] Torchia, D.A. and Szabo, Attila., J. Magn. Reson. 49, 107 (1982).

[47] Bloembergen N., Purcell, E.M. and Pound, R.V., Physical Rev. 73, 679 (1948).

[48] Lee, JeongYong., Farha, Omar. K., Roberts, John., Scheidt, Karl. A., Nguyen, SonBinh. T. and Hupp, Joseph. T., Chem. Soc. Rev. 38, 1450 (2009).

[49] Allendorf, Mark. D., Schwartzberg, Adam., Stavila, Vitalie. and Talin, A. Alec., Chem. Eur. J. 17, 11372 (2011).

[50] Horcajada, Patricia., Serre, Christian., Maurin, Guillaume., Ramsahye, Naseem. A., Balas, Francisco., Vallet-Regi, Maria., Sebban, Murial., Taulelle, Francis. and Ferey, Gerard., J. Am. Chem. Soc. 130, 6774 (2008).

[51] Auerbach, Scott. M., Bull, Lucy, M., Henson, Neil. J., Metiu, Horia. I. and Cheetham, Anthony. K., J. Phys. Chem. 100, 5923 (1996).

[52] Bull, Lucy. M., Henson, Neil. J., Cheetham, Anthony. K., Newsam, John. M. and Heyes, Stephen. J., J. Phys. Chem. 97, 11776 (1993).
[53] Gonzalez, Jorge., Devi, R. Nandini., Tunstall, David. P., Cox, Paul. A. and Wright, Paul. A., Microporous and Mesoporous Mater. 84, 97 (2005). 97-104

[54] Kolokov, D.I., Stepanov, A.G., Guillerm, V., Serre, C., Frick, B. and Jobic, H., J. Phys. Chem. C 116, 12131 (2012).

[55] Kolokov, D.I., Jobic, Herve., Stepanov, Alexander. G., Guillerm, Vincent., Devic, Thomas., Serre, Christian. and Ferey, Gerard., Angewandte. Chemie. 122, 4901 (2010).

[56] He, Ming., Yao, Jianfeng., Liu, Qi., Zhong, Zhaoxiang. and Wang, Huanting., Dalton Trans 42, 16608 (2013).

[57] Carvillon, Janosch., Schroder, Christian. A., Bux, Helge., Rothkirch, Andre., Caro, Jurgen. and Wiebcke, Michael., Cryst. Eng. Comm. 14, 492 (2012).

[58] Jelinski, L.W., Methods and Stereochemical Analysis 7, 335 (1986).

[59] Macho, V., Brombacher, L. and Spiess, H.W., Appl. Magn. Reson. 20, 405 (2001).

[60] Singh, Ajay. Kumar. and Mehrotra, N.K., Indian J. Pure & Appl Phys. 43, 39 (2005).

[61] Karge, H.G. and Weitkamp, J., *Adsorption and Diffusion*, Springer-Verlag Berlin Heidelberg, 2008.